PLS-II 빔라인 소개 및 X-선 광학계 기초

미래기반 가속기
전문인력양성 사업단

Materials Today Physics 6 68(2018)

Sept. 17 2022

Ki-jeong Kim
Pohang Accelerator Lab., Korea
kjkim@postech.ac.kr

미래기반 가속기 전문인력양성 사업단

- **Beamline and Experiments**

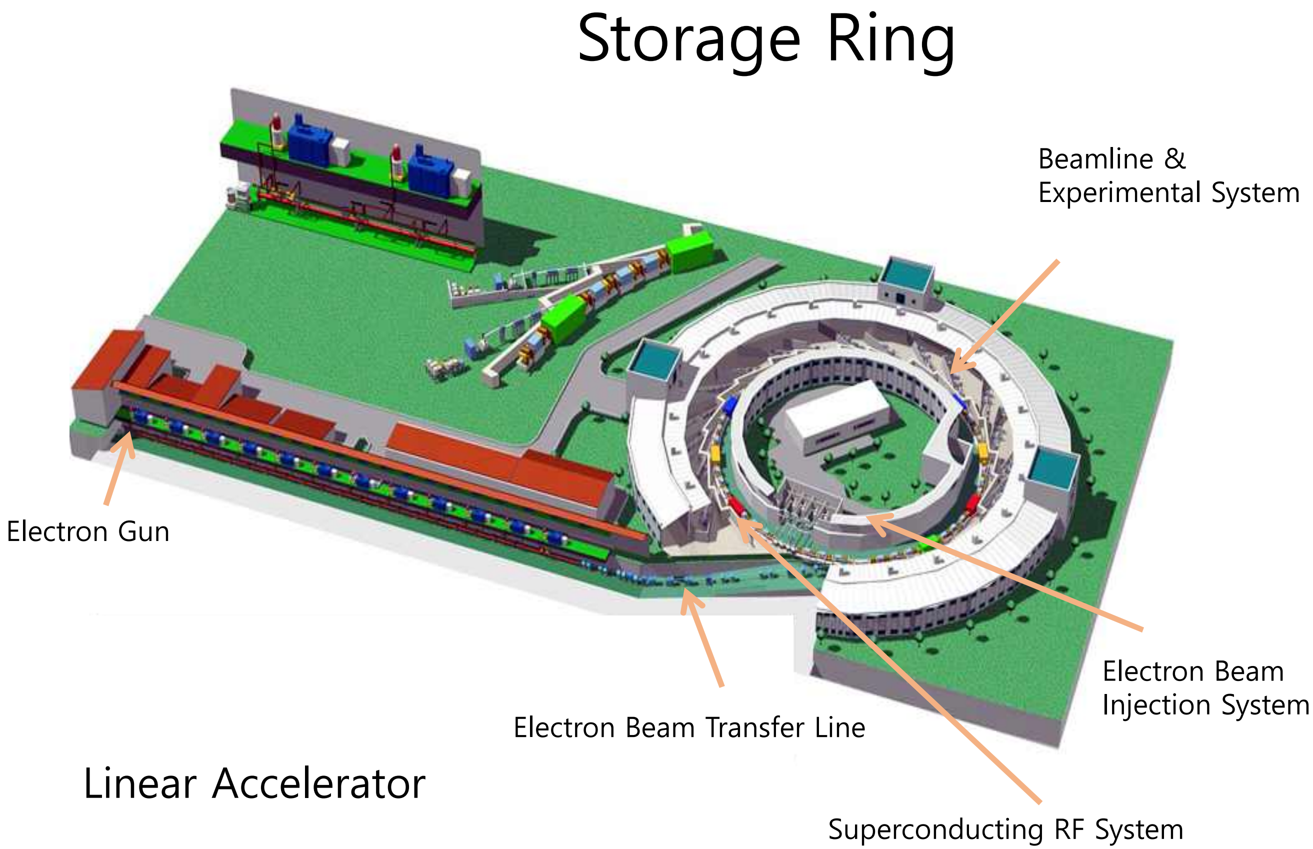

http://pal.postech.ac.kr

History of Synchrotron Radiation

PLS-I	PLS-II	PAL-XFEL	Korea-4GSR
E = 2.5GeV I = 200mA	E = 3GeV I = 300mA (max. 400mA)	XFEL E = 10 GeV Beam Charge=0.2nC	E = 4GeV I = 400mA
1994	2012	2017	2030

The discovery of radiation → 1st Gen → 2nd Gen → 3rd Gen → 4th Gen → 5th Gen

1946

The first discovery of synchrotron radiation in a 70 MeV accelerator for particle physics research

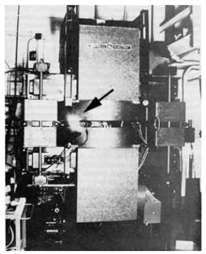

at General Electric(1946)

1960s

The parasitic use of synchrotron radiation from accelerators originally designed for particle physics research

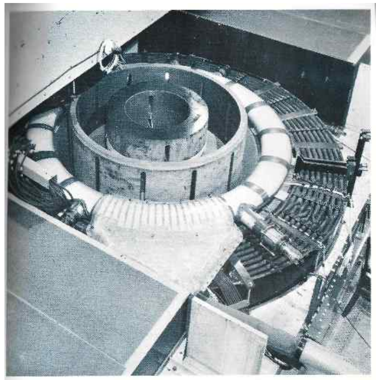

SURF(1966)

- SURF (USA)
- CHESS (USA)
- DESY (Germany)
- SOR (Japan)

1980s

Production of synchrotron radiation dedicated solely to experiment with bending magnet

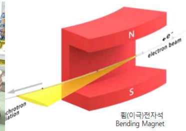

2nd Gen. Bending Magnet

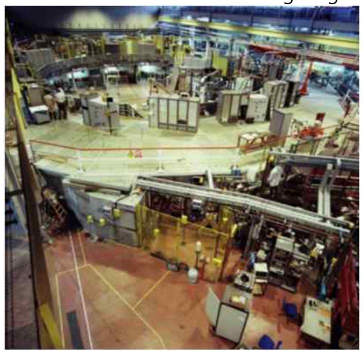

SRS at Daresbury Laboratory(1980)

- NSLS (USA)
- Photon Factory (Japan)
- MAX-I (Sweden)

1990s

Introducing "undulators" and "wigglers" to produce more powerful synchrotron radiation

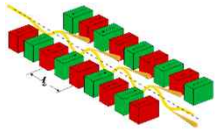

3rd Gen. Undulator

PLS-II (2012)

- PLS-II (South Korea)
- ESRF (Europe)
- APS (USA)
- SPring-8 (Japan)

*Including above, a total of 37 Synchrotron facilities are currently in operation or under construction worldwide.

2016 ~

From rearranging magnet lattice, generation of brighter, smaller and more coherent synchrotron radiation

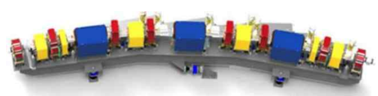

3rd Gen. Magnet Lattice

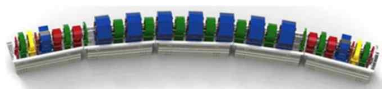

4th Gen. Magnet Lattice

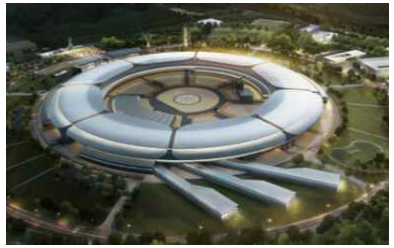

Korea-4GSR(under construction)

- MAX IV
- ERSF-EBS
- SIRIUS

Future

What's Next?

Major Parameter of PLS-II

Parameter	Value
Beam energy	3 GeV
Beam current	360 mA(Max. 400 mA), Top-up mode
Lattice structure	Double-Bend
Super-period	12
Emittance	5.8 nmrad
Tune(H/V)	(15.375/9.145)
RF frequency	499.96 MHz
Energy spread	0.1%

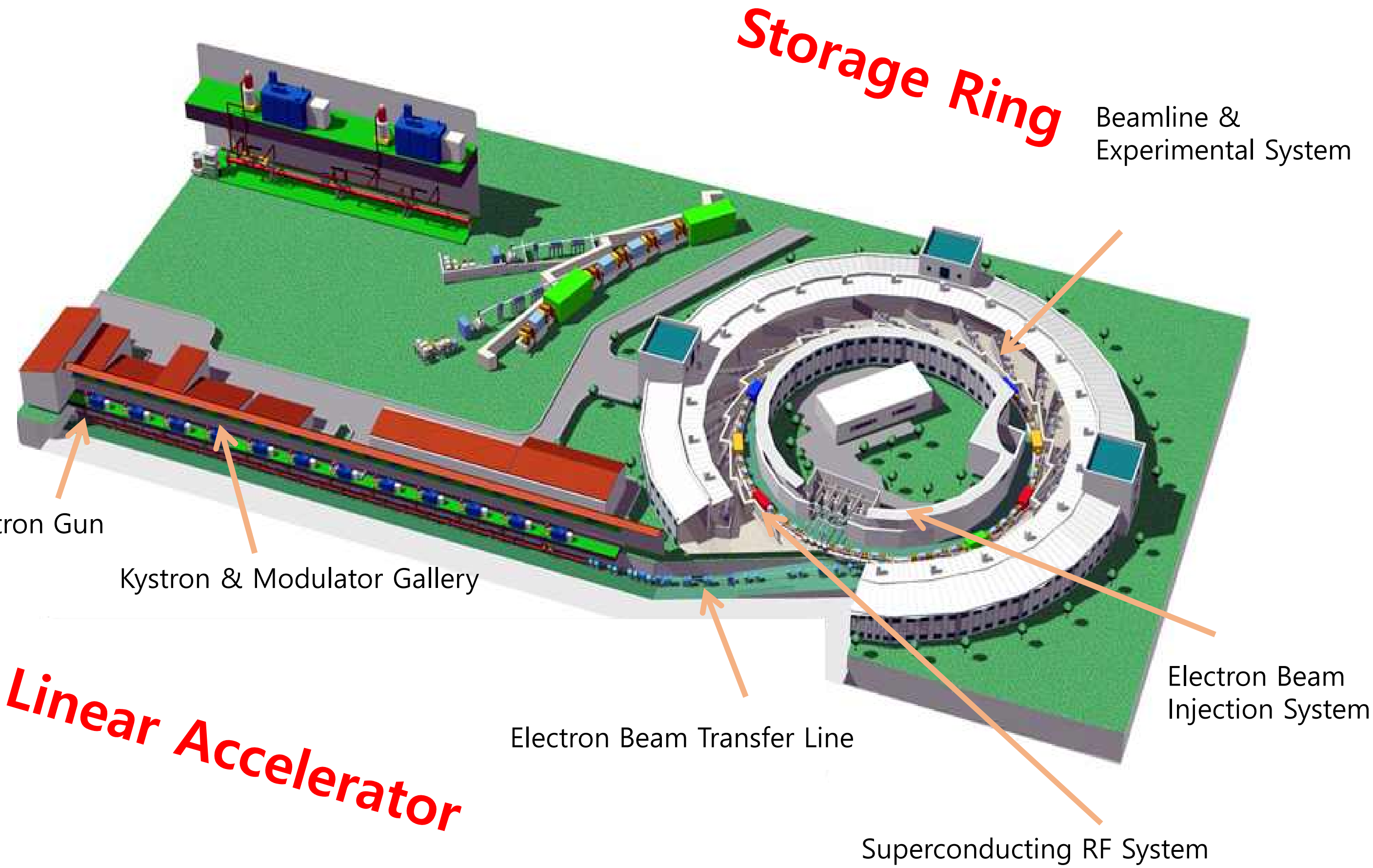

Three Forms of Synchrotron Radiation

미래기반 가속기
전문인력양성 사업단

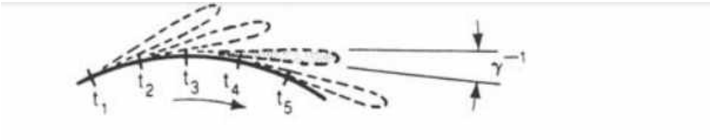

Bending Magnet-A sweeping Searchlight"

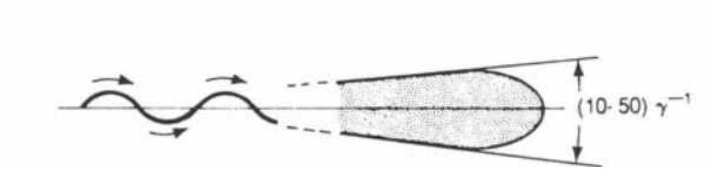

Wiggler – Incoherent Superposition

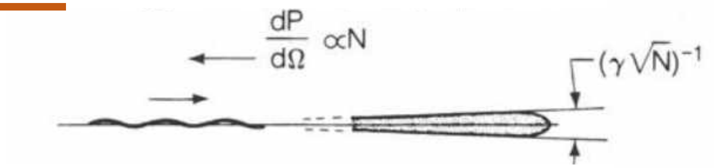

Undulator – Coherent Interference

$$\frac{dP}{d\Omega} \propto N^2$$

$$\Omega \propto \frac{1}{N}$$

$$P \propto N$$

N = number of magnetic periods (~100)

$$\gamma^{-1} = \frac{m_o c^2}{E_e} = \frac{0.511}{E_e(\text{GeV})} \text{ mrad}$$

Deflection parameter K

$$K = \frac{eB_0\lambda_u}{2\pi m_e c}$$

$$=0.934 B_0[\text{Tesla}]\lambda_u[\text{cm}]$$

K>>1

K>1

0.170 mrad(@ PLS-II)

1.665 keV(@ PLS-II)

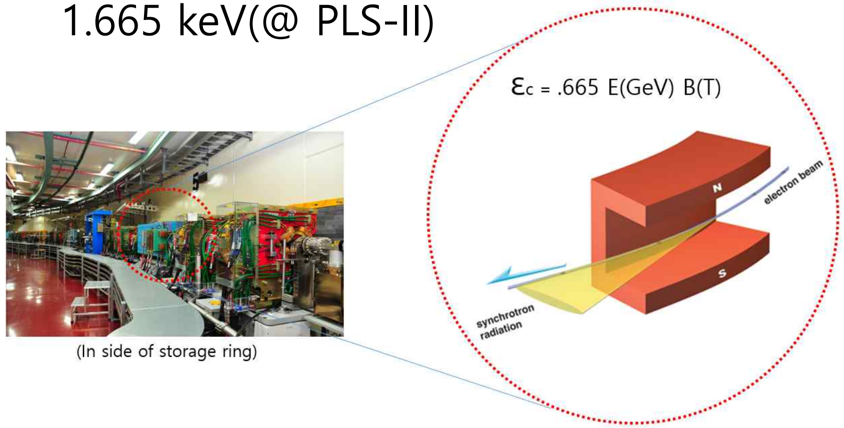

(In side of storage ring)

$$\varepsilon_n[\text{keV}] = \frac{0.949 n E^2[\text{GeV}]}{\lambda_u[\text{cm}]}\left(\frac{1}{1+K^2/2+\gamma^2\theta^2}\right)$$

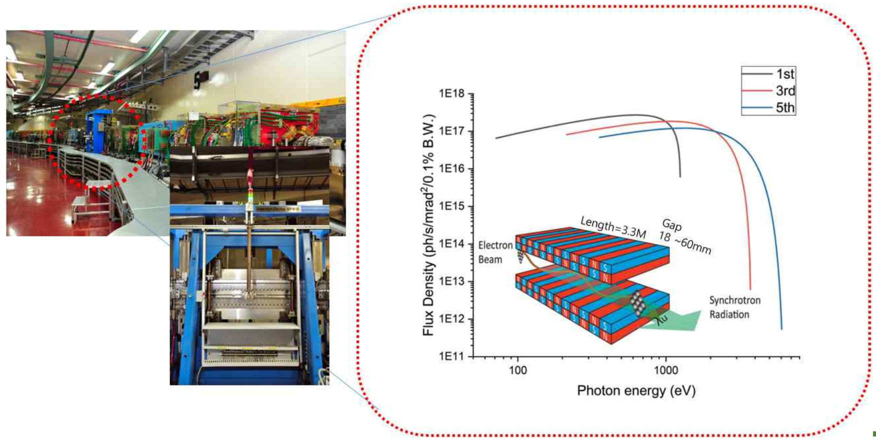

Synchrotron Radiation Produced by BM and Undulators

미래기반 가속기 전문인력양성 사업단

$$\gamma = \frac{E_e}{mc^2} = 1957\, E_e(\mathrm{GeV})$$

ε_c = .665 E(GeV) B(T)

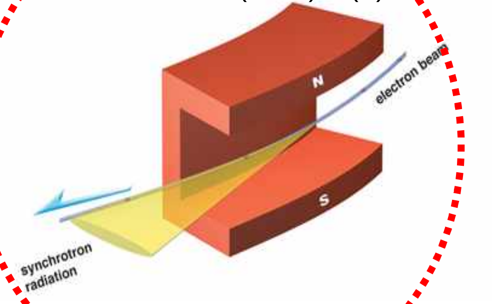

Bending magnet

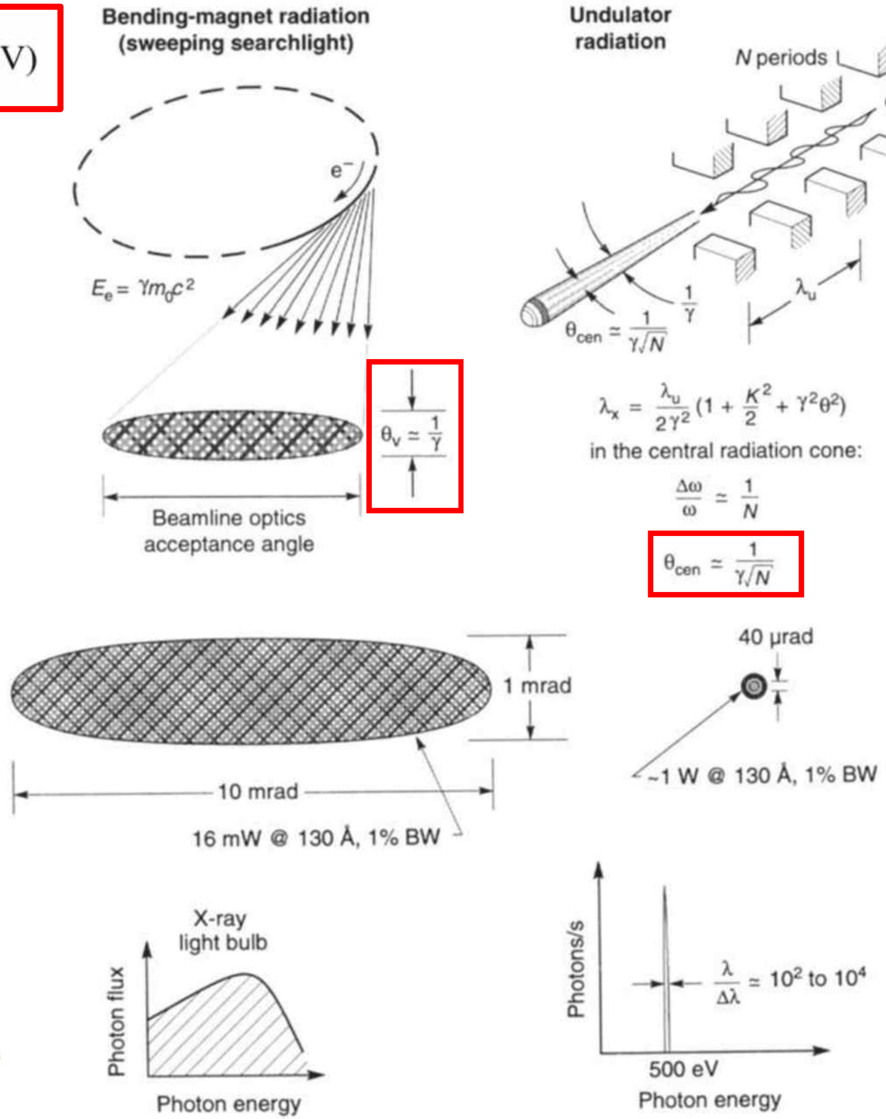

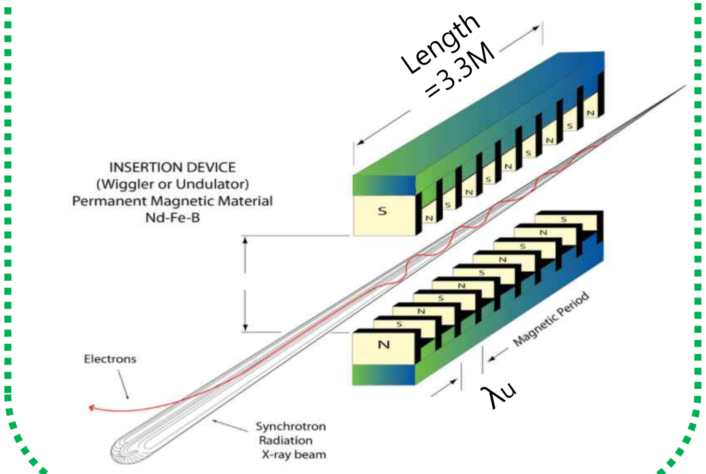

Undulator

Characteristics of Synchrotron Radiation

미래기반 가속기
전문인력양성 사업단

- *Very high brightness(high spatial resolution, high spectral resolution)*
- *Tunability*
- *High degree of coherence*
- *A pulsed nature*
- *Linear circular polarization*
- *High flux*

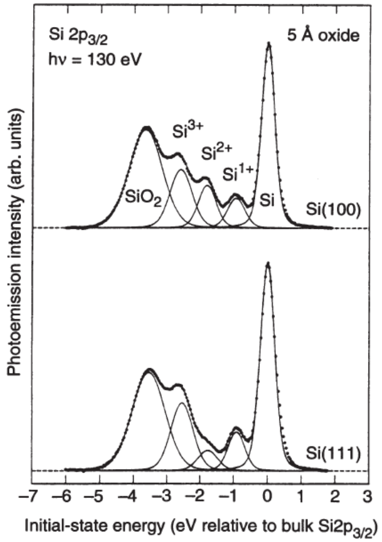

Figure 19. Photoemission from Si(100) with a 5-Å oxide surface, shown as a function of initial-state energy. The oxidation states of Si are shown to be resolved. From Himpsel, McFeely, Taleb-Ibrahimi, Yarmoff, and Hollinger, Physical Review B **38**, 6084 (1988). (Measurements made at the National Synchrotron Light Source.)

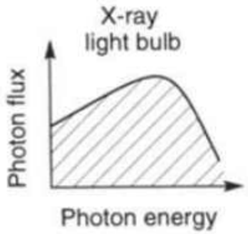

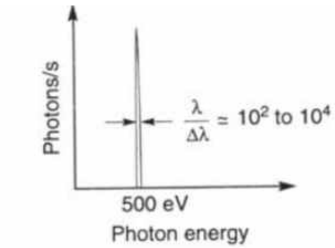

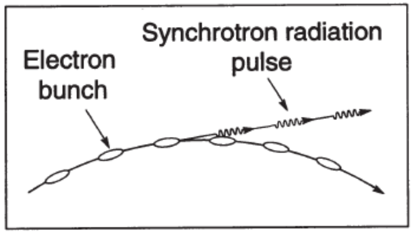

Figure 13. Schematic illustration of the bunched structure of an electron beam circling in a storage ring and the corresponding pulsed nature of the synchrotron radiation. At the ALS, for example, 250 electron bunches circle the ring. Each has a duration of about 35 picoseconds. The spacing between bunches, dictated by the rf frequency, is 2 nanoseconds.

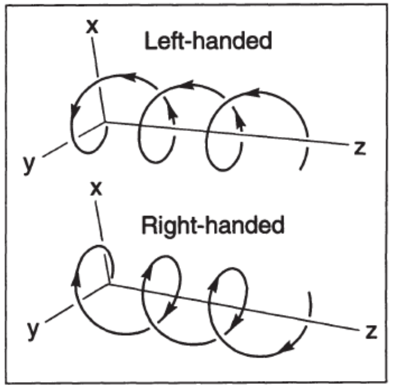

Figure 25. The unique property of circularly polarized light is the spiral path of its electric-field component. This component maps out a clockwise or counterclockwise circular path to form a right-handed or left-handed spiral.

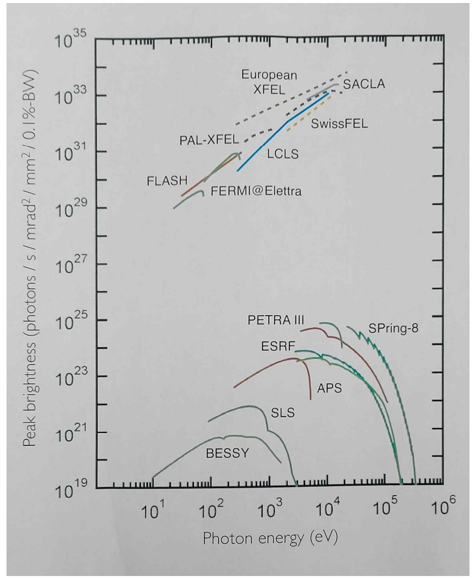

Beamlines

미래기반 가속기
전문인력양성 사업단

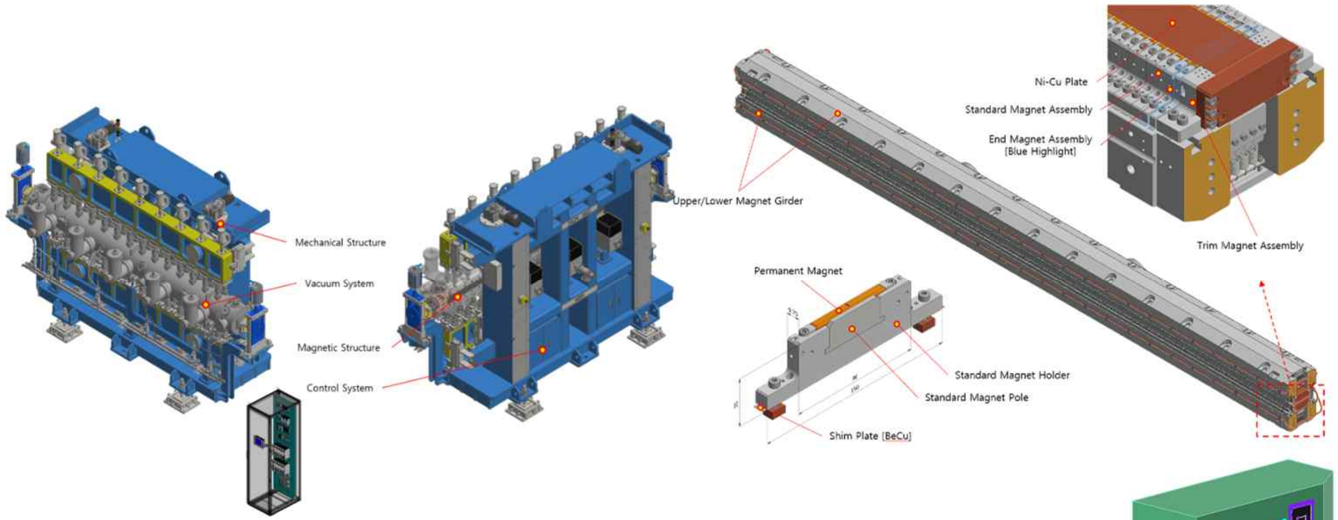

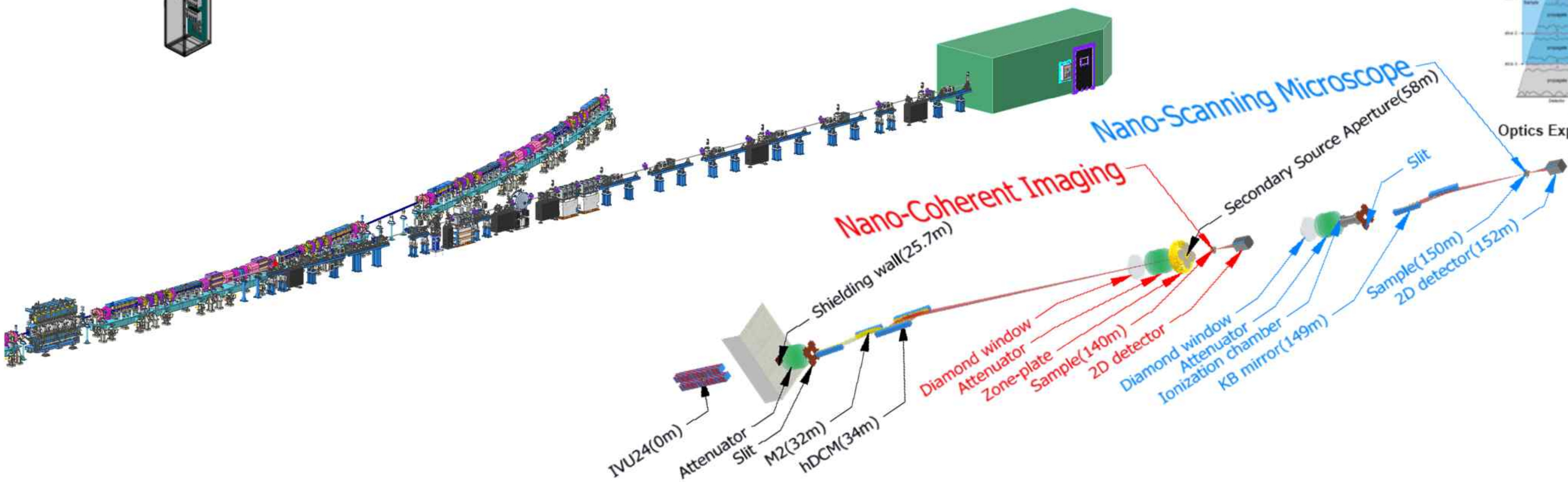

Near-field ptychography

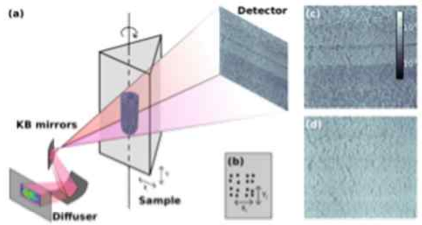

Optics express 23.10 (2015): 12720-12731.

Multi-slice ptychography

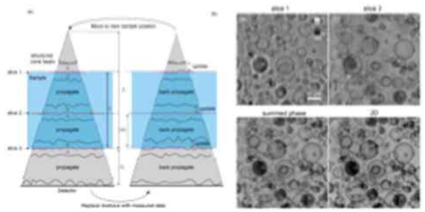

Optics Express 31.10 (2023): 15791-15809.

PLS-II Beamline Map

미래기반 가속기
전문인력양성 사업단

포항가속기연구소 과학기술정보통신부

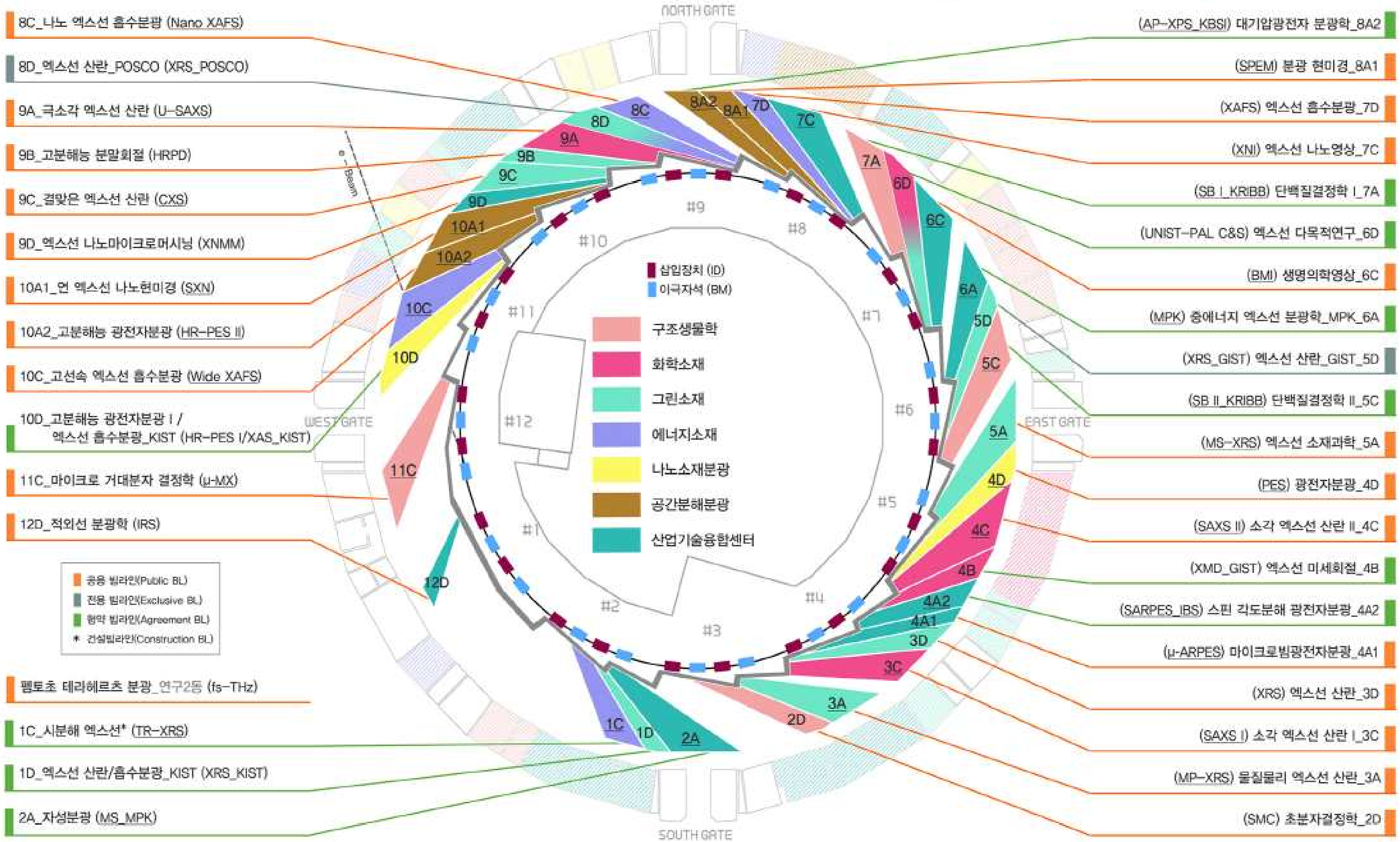

Researchers using Synchrotron Radiation

- ✓ VUV/Soft X-ray
- ✓ Hard X-ray

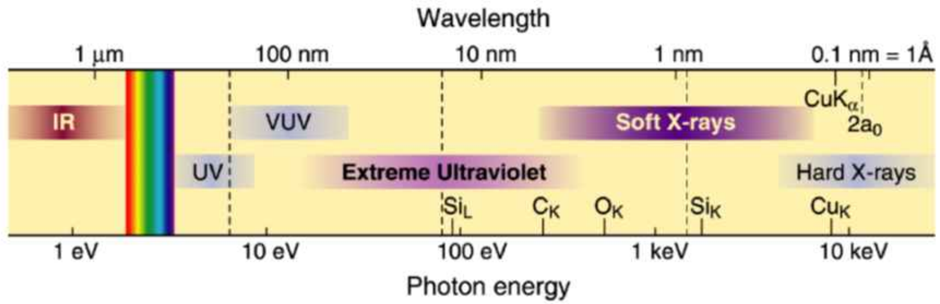

VUV/Soft X-ray	Hard X-ray
What are the electrons doing as they migrate between the atoms?	Where are the atoms?
Chemical bonding Valence band structure	Determination crystal structure and molecular structure
Photoelectron λ_{el} = 1 Å	Photon λ_{ph} = 1 Å
E (electron) = $p^2/(2m)$ = $h^2/(2m\lambda_{el}^2)$ ∽ 150 eV. * De Brogile wavelength λ=h/p	E (photon) = hc/λ_{ph} ∽ 12.4 keV.

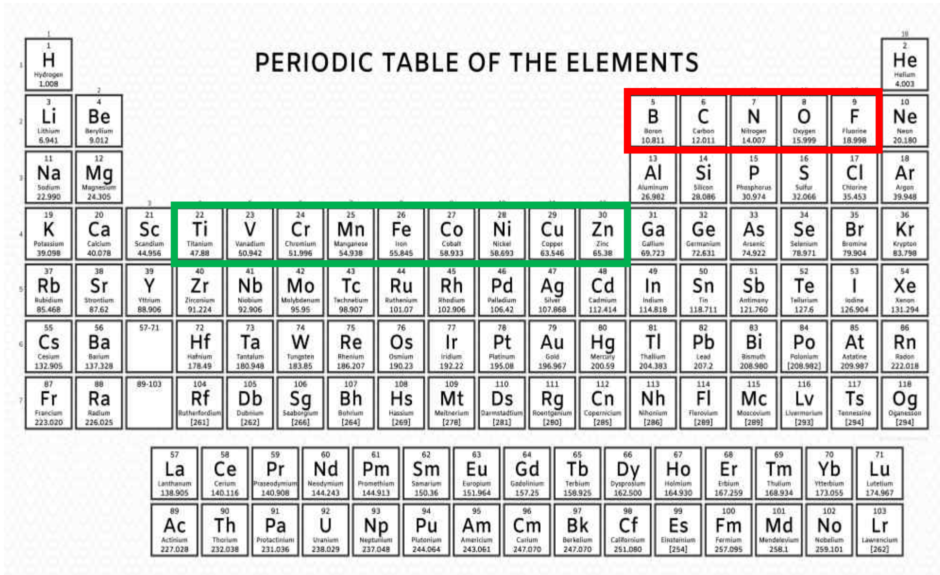

Neville Smith, Phys. Today, 2005

Absorption-edge energies of the elements

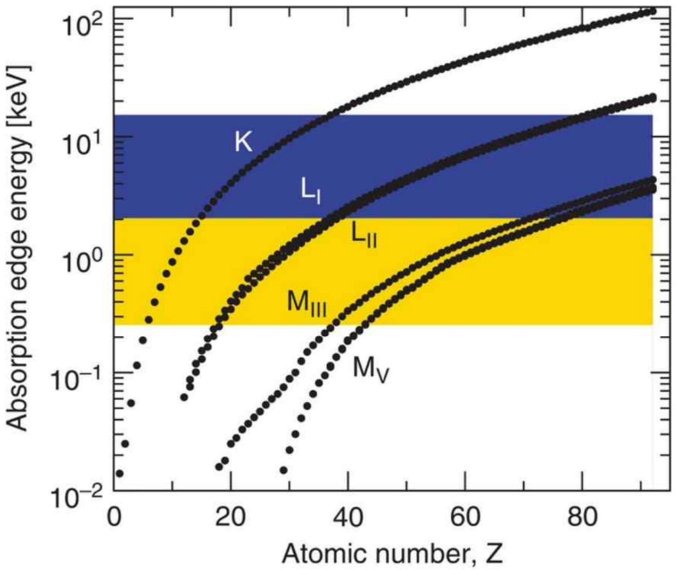

Figure 7.28 Absorption-edge energies of the elements between hydrogen and uranium. Soft x-ray RIXS machines cover approximately the energy regime highlighted in yellow, hard x-ray RIXS equipment the range in blue.

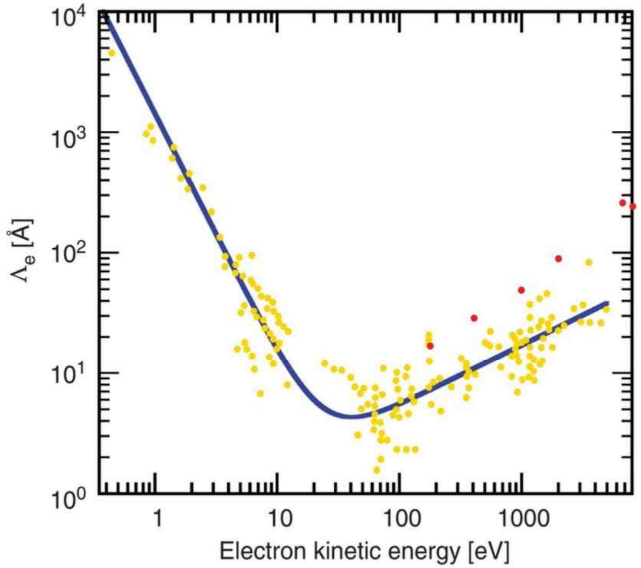

Figure 7.9 The universal curve. Plot of the inelastic mean free path (IMFP) of electrons emerging from the surface of condensed matter, as a function of electron kinetic energy $\mathscr{E}_e$. The solid blue line describes the general expression $\Lambda_e = A/\mathscr{E}_e^2 + B\sqrt{\mathscr{E}_e}$, encapsulating both the low-energy (below 15 eV) and high-energy (above 150 eV) limiting physical cases. The best least-squares fit results in $A = 1430$ and $B = 0.54$ if $\mathscr{E}_e$ is expressed in eV. The yellow points are experimentally determined values, mainly from elemental samples. The red points are for water, important data for solid–liquid-interface data in high-pressure XPS experiments. Adapted from [3] with permission from John Wiley.

Layout of Beamlines(8A)

Front End

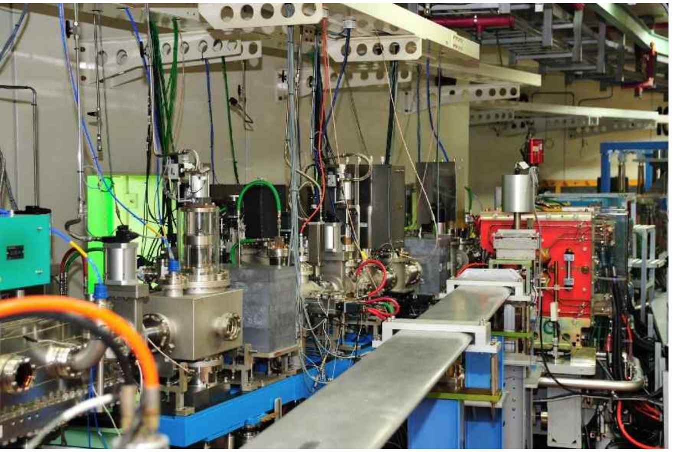

X-ray Beamline

Soft X-ray Beamline

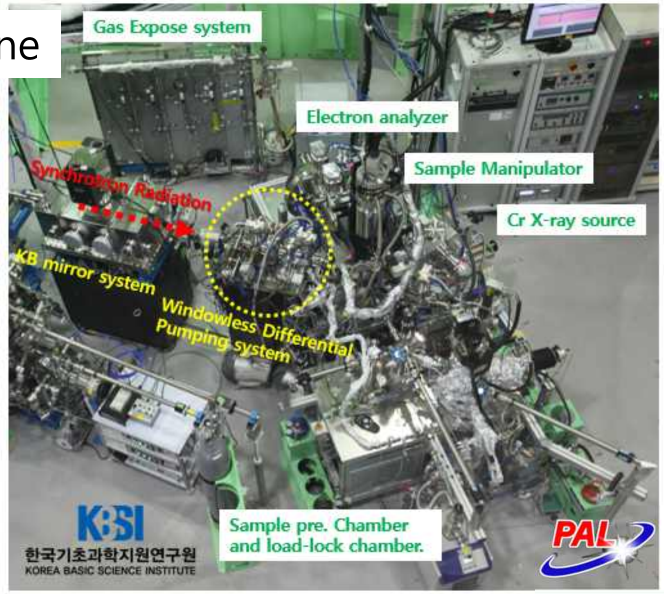

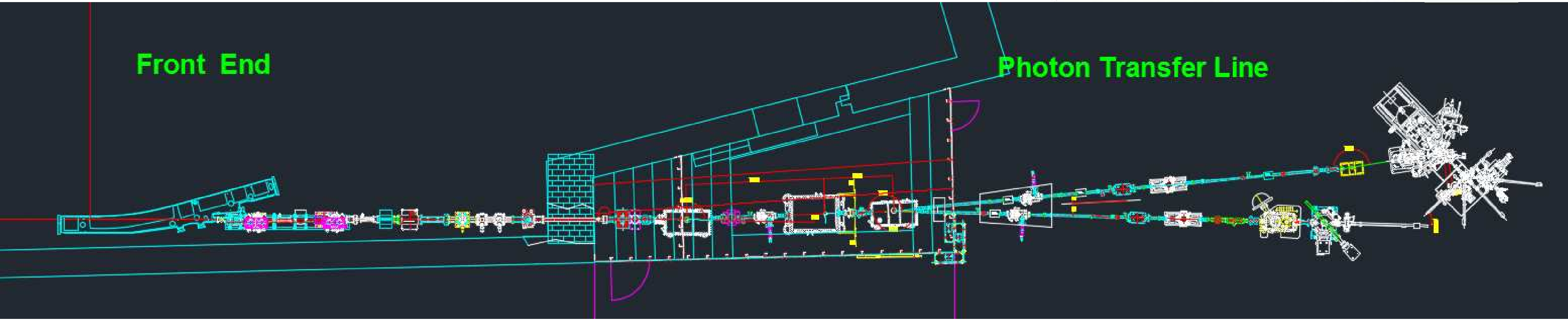

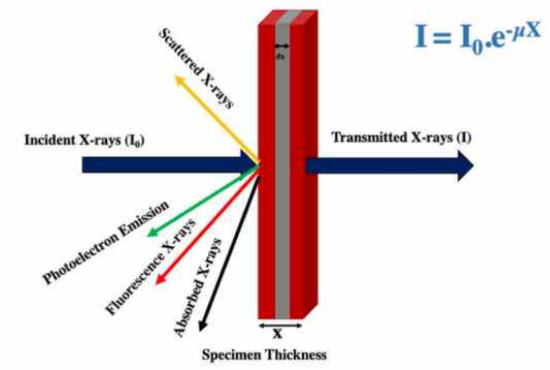

https://www.researchgate.net/publication/344196119_Physical_Methods_for_LiNa_Ion_Battery_Characterization

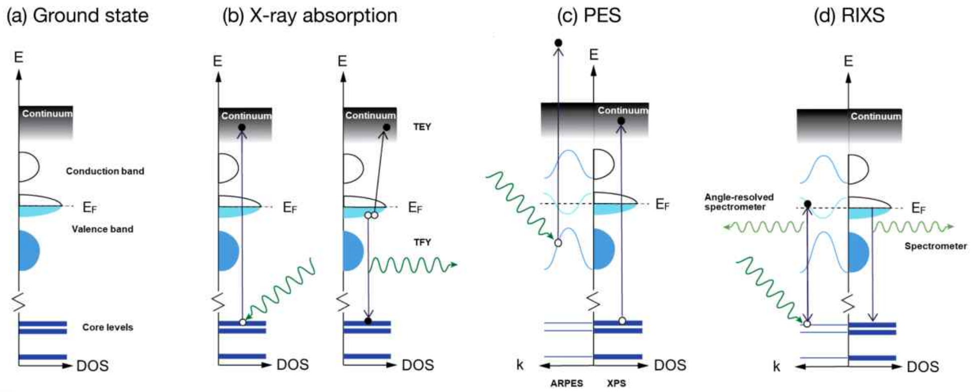

J. Appl. Phys. 129, 220902 (2021)

Photoemission Spectroscopy

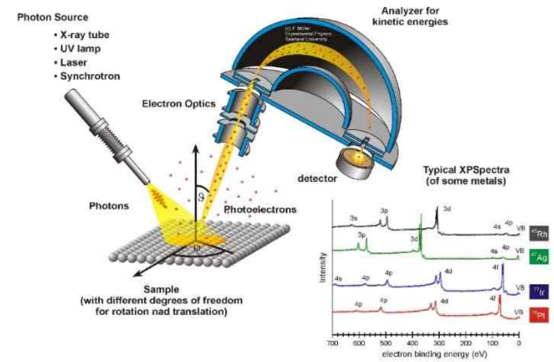

X-ray Absorption Spectroscopy

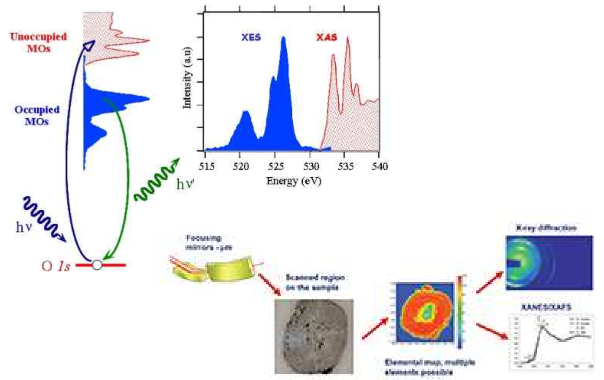

X-ray Scattering

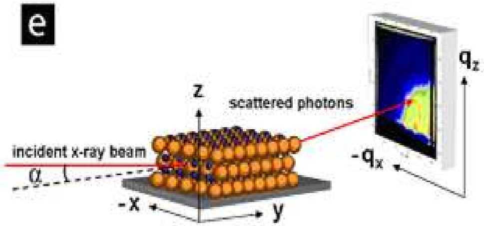

X-ray Imaging

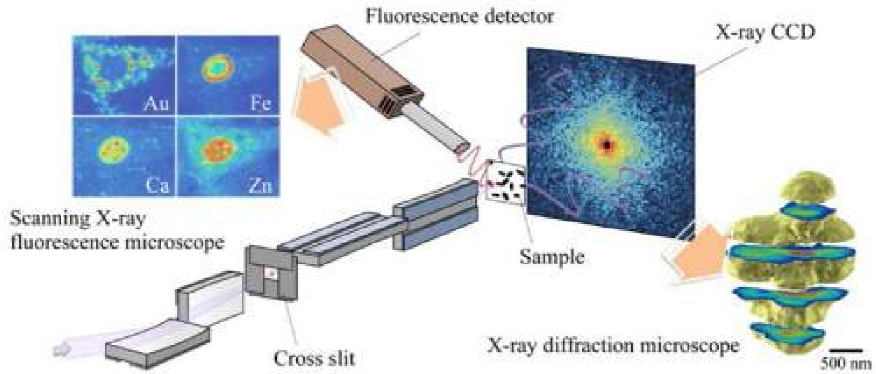

A Typical X-ray Beamline

미래기반 가속기
전문인력양성 사업단

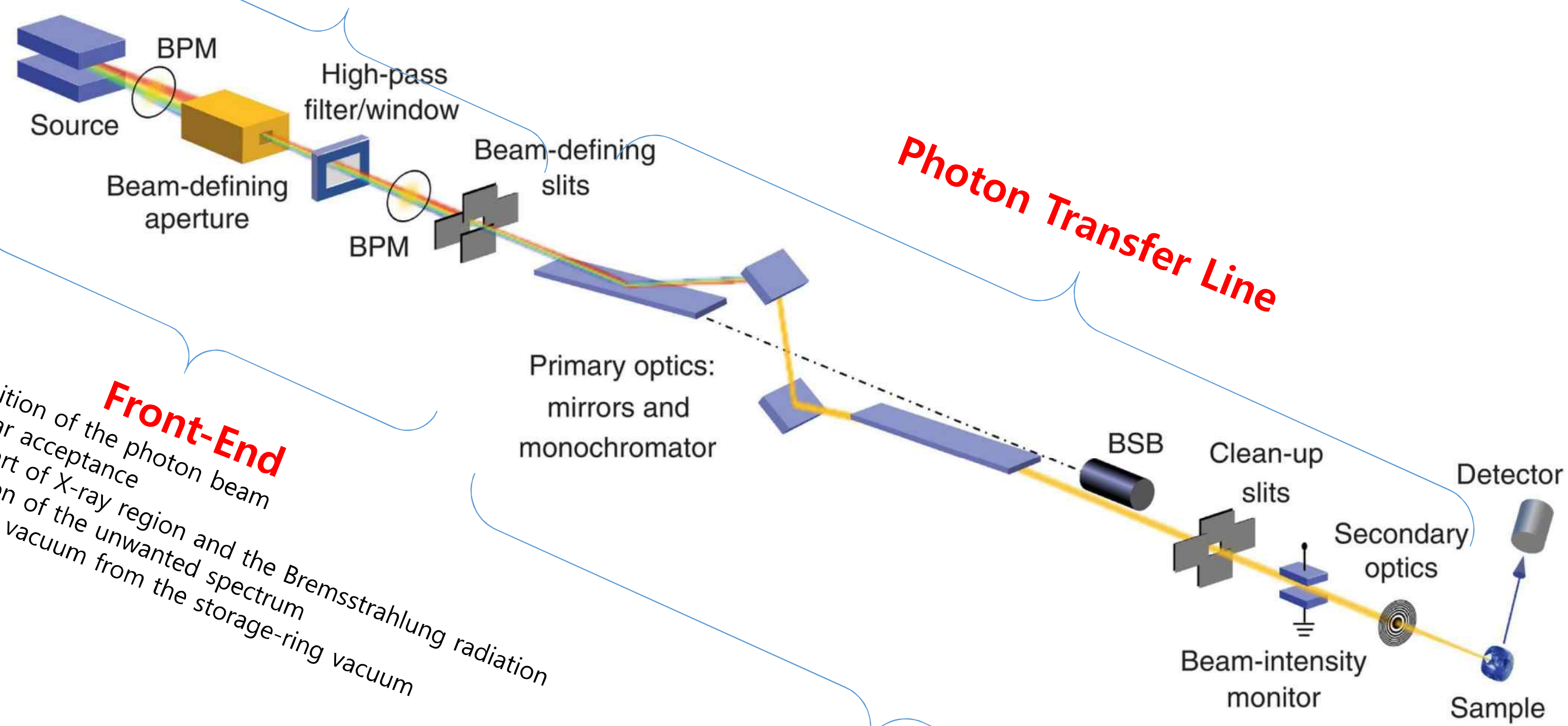

- Monitor the position of the photon beam
- Define the angular acceptance
- Block the some part of X-ray region and the Bremsstrahlung radiation
- Filter out the portion of the unwanted spectrum
- Isolate the beamline vacuum from the storage-ring vacuum

Figure 5.1 Typical components found at an x-ray synchrotron beamline. BPM = beam-position monitor. By installing two or more BPMs, both the beam height and the tilt angle can be determined. BSB = Bremsstrahlung blocker. The precise nature of each component can vary significantly from beamline to beamline, while not all components shown here are necessarily used.

An Introduction to Synchrotron Radiation: Techniques and Applications, Second Edition. Philip Willmott.

WILEY

Optical devices and Vacuum system

미래기반 가속기
전문인력양성 사업단

✓ **Making the emitted photon suitable for practical experiments : Optical devices**

✓ **Deliver meaningful photon flux to Exp. Station : Vacuum system**

❖ **Absorption lengths for X-rays in gases**

Gas	hv		
	1 keV	3 keV	10 keV
Hydrogen	1.52 m	19.8 m	28.86 m
Helium	0.85 m	29.56 m	286 m
Nitrogen	0.236 m	5.38 m	1.739 m

❖ **Absorption lengths for Be**

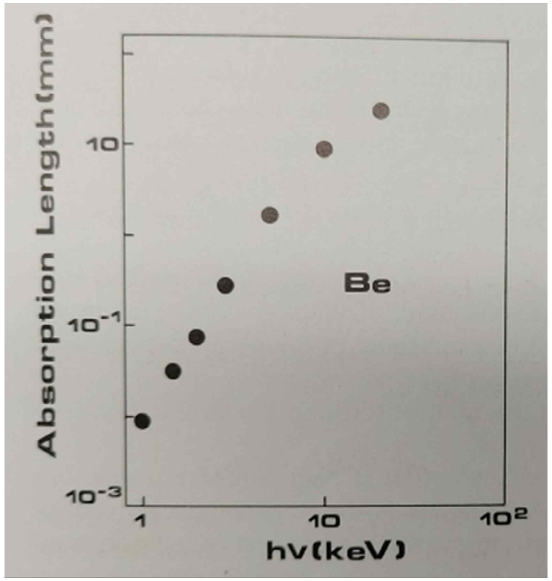

✓ **Transmission optics for synchrotron radiation is difficult(or impossible).**

Beam-position monitor(BPM)

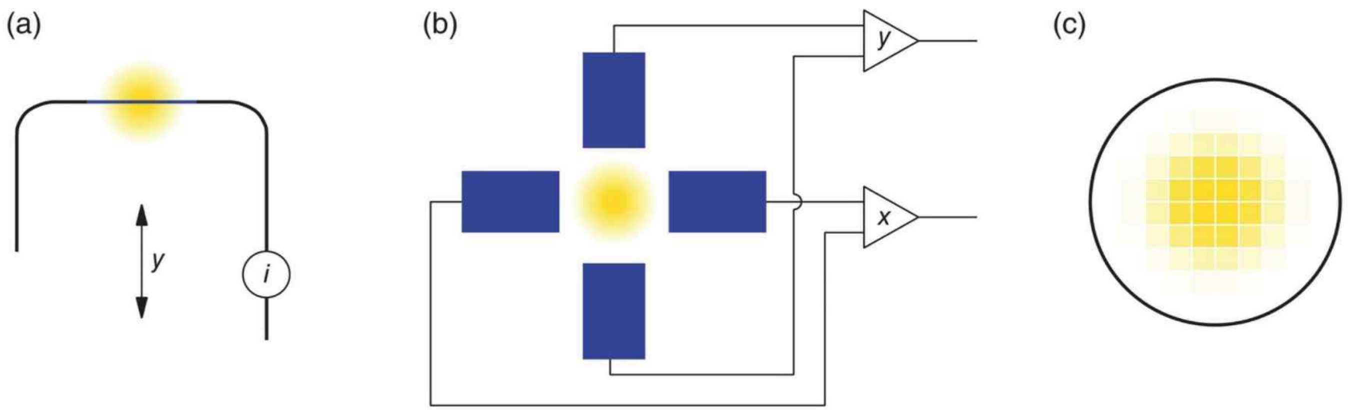

Figure 5.2 Different designs for beam-position monitors: (a) a simple 1D wire monitor, (b) a 2D blade monitor, and (c) a diamond CVD profile monitor.

Beam-position monitor(BPM)

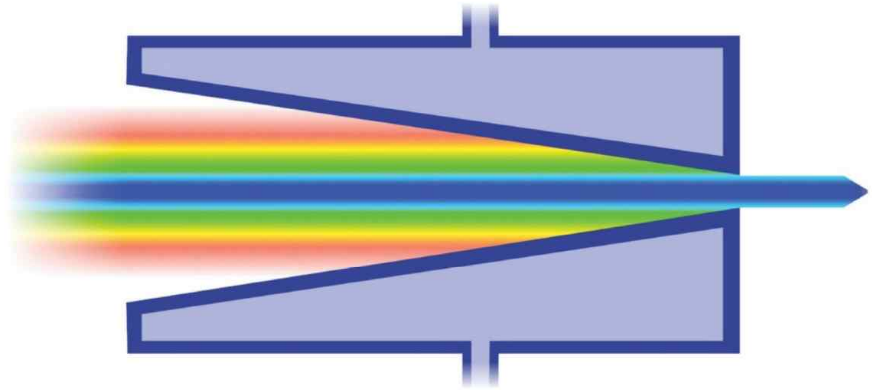

Figure 5.3 Beam-defining primary apertures. Normally the first component downstream of the source, these water-cooled apertures define the angular range to the beamline and often have a rectangular cone shape, in order to distribute the thermal load over a larger area. Because the outer parts of the synchrotron radiation contains lower-energy photons than the central cone, these apertures also act as high-pass filters.

An Introduction to Synchrotron Radiation: Techniques and Applications, Second Edition. Philip Willmott.

High-pass filter

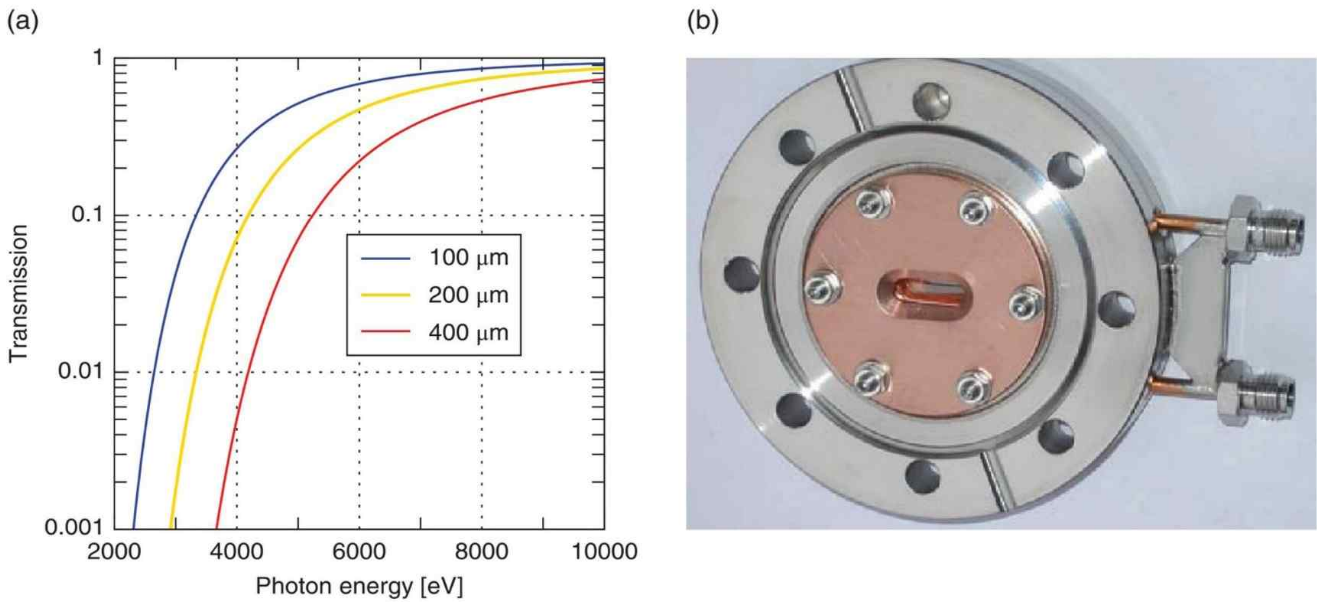

Figure 5.4 High-pass diamond front-end filters used to remove the low-energy component of the x-ray spectrum. (a) The transmission curves for various thicknesses of diamond filters, assuming a density of 3.5 g cm^{-3}. (b) A 100 μm-thick, ultra-high-vacuum-compatible, water-cooled diamond window, used to remove soft x-rays and provide isolation between the storage-ring vacuum and the beamline vacuum. Courtesy of Max Kleeb, Paul Scherrer Institute.

Available x-ray optical techniques

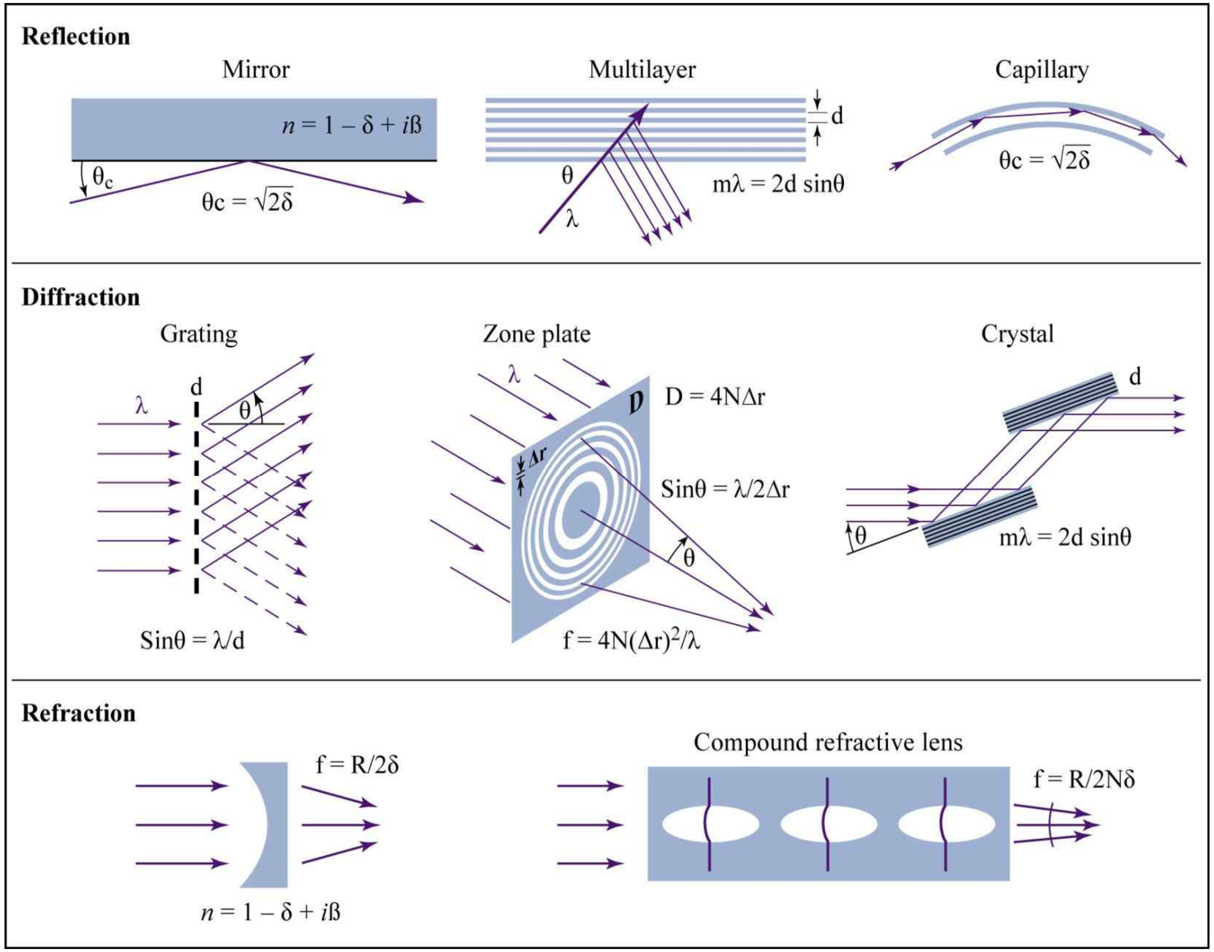

Soft X-rays and extreme ultraviolet radiation, David Attwood(2016)

A Fresnel zone plate lens   multilayer-coated two-bounce Schwarzschild   multilayer Laue lens   Full-field TXM

KB

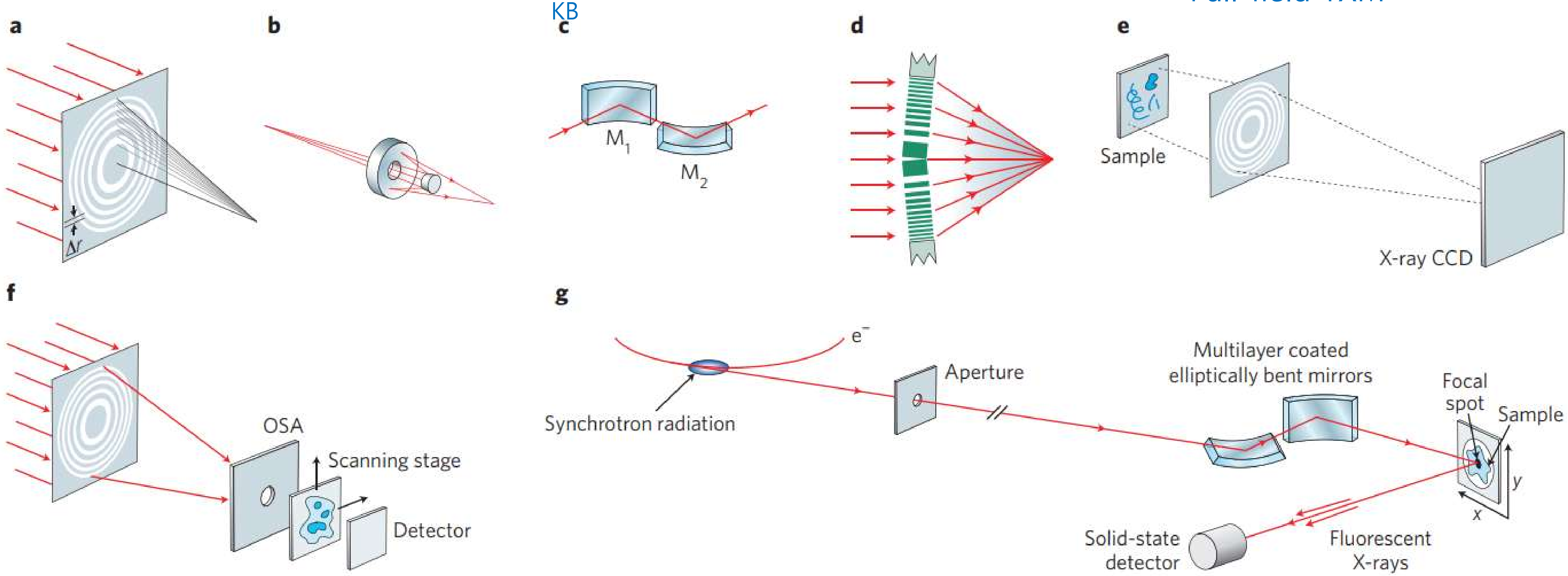

Zone-plate-based STXM

N. Photonics, 4 840(2010)

Mirrors for Synchrotron Beamlines

미래기반 가속기
전문인력양성 사업단

- ✓ **Reflect**
- ✓ **Focusing**
- ✓ **Harmonic Rejection(filter ultra-violet and X-ray)**
- ✓ **Power Reduction**

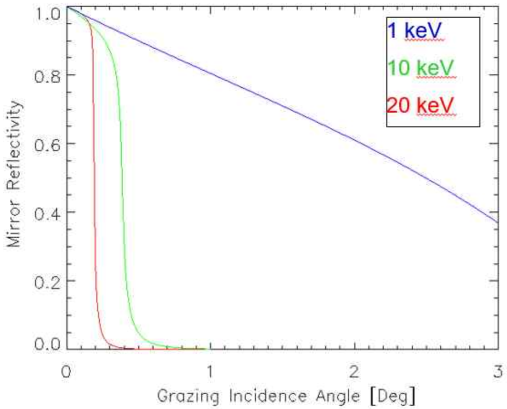

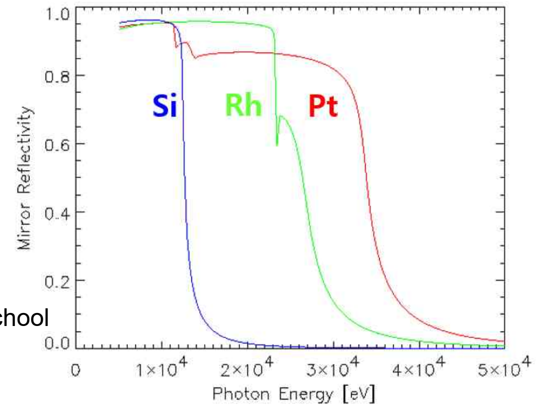

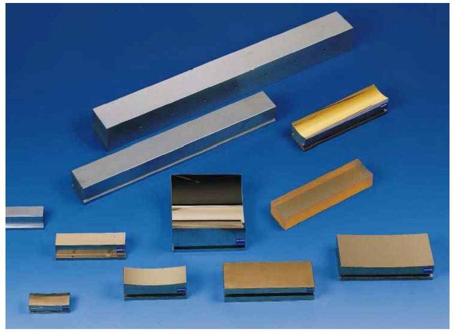

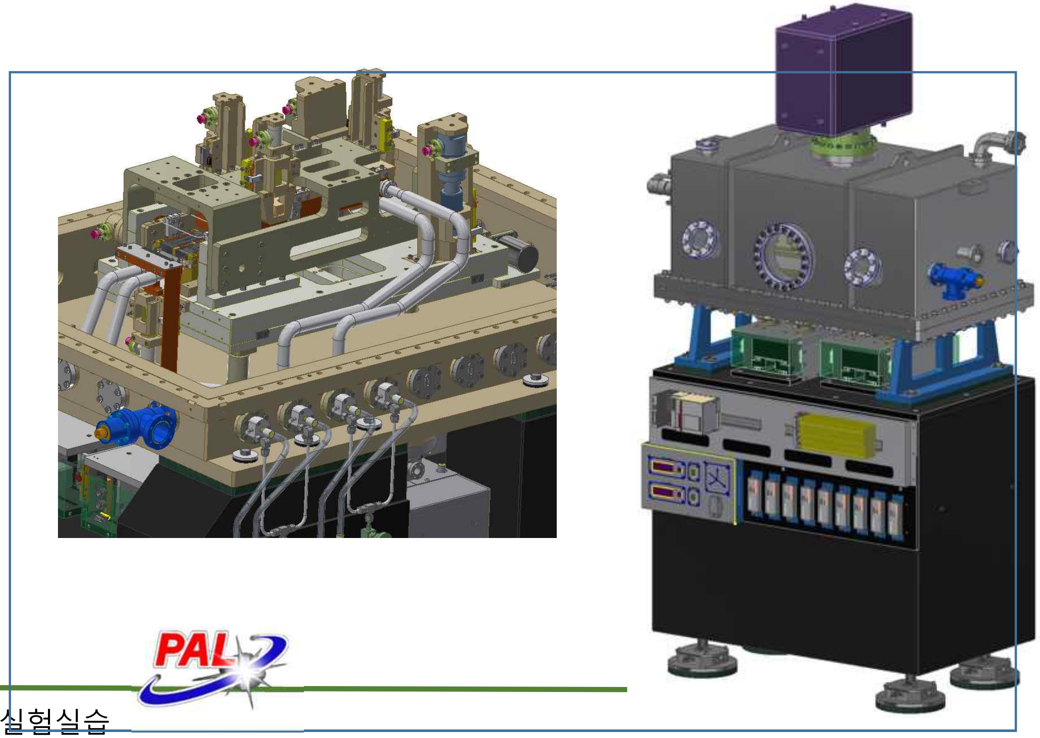

R. Garrett 1st AOF Synchrotron School

X-ray Mirrors for Synchrotron Beamlines

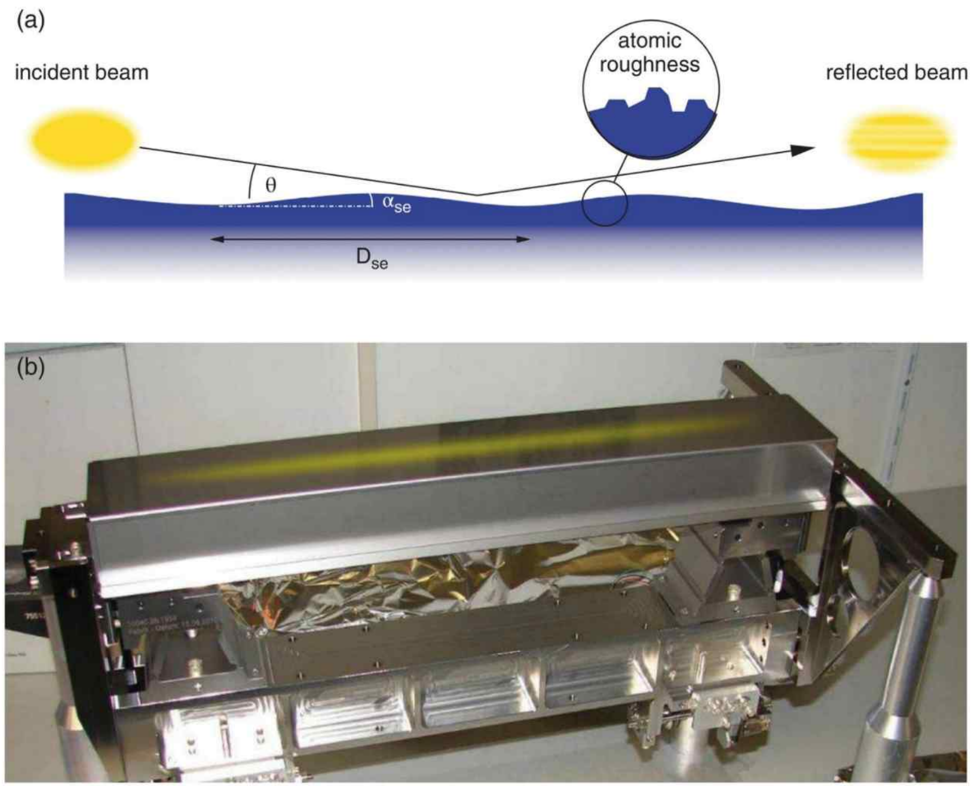

Figure 5.17 X-ray mirrors. (a) A reflecting flat x-ray mirror has a residual mesoscopic/macroscopic 'wobbliness' to it, referred to as the slope error, which causes the beam profile to become more irregular. In addition, the roughness on an atomic scale must not exceed a few angstroms. (b) A bendable silicon mirror at the Materials Science beamline. The usable length is 400 mm. The footprint of the grazing-incidence beam is shown as the narrow yellow ellipse. Courtesy Dominik Meister, Paul Scherrer Institute.

An Introduction to Synchrotron Radiation: Techniques and Applications, Second Edition. Philip Willmott.

Different Monochromator Type

미래기반 가속기
전문인력양성 사업단

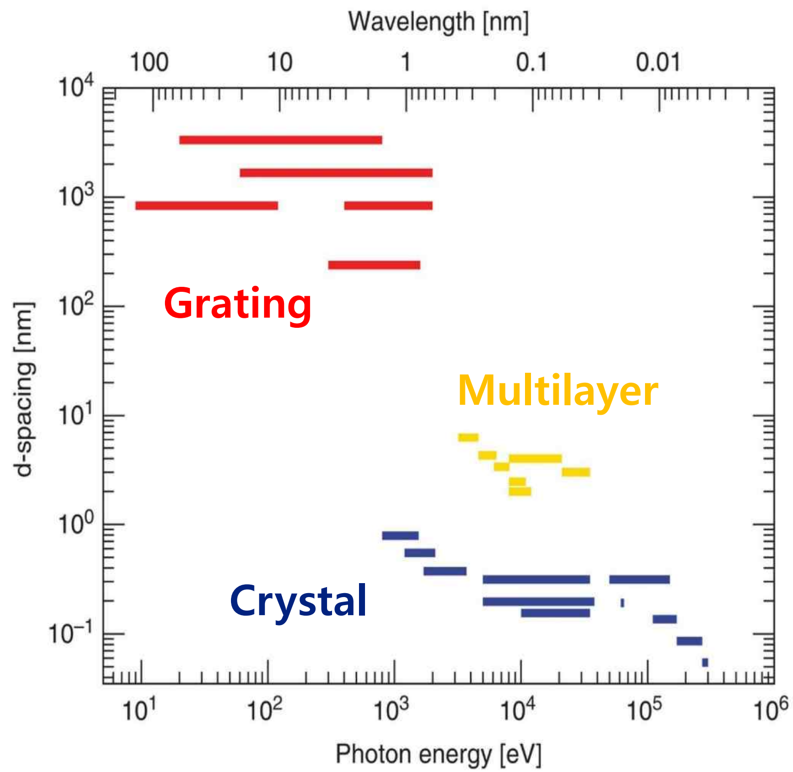

Figure 5.20 Different monochromator types. A selection of grating (red), multilayer (yellow), and crystal (blue) monochromator element periodic spacings *d* and the typical energy range that they serve.

An Introduction to Synchrotron Radiation: Techniques and Applications, Second Edition. Philip Willmott.

WILEY

Monochromators: Crystals and Gratings

- ✓ Diffraction from periodic structures is used to select the desired energy from the "white" synchrotron radiation.
- ✓ Crystals used at hard X-ray energies Bragg's law:

$$2d\sin\theta = m\lambda$$

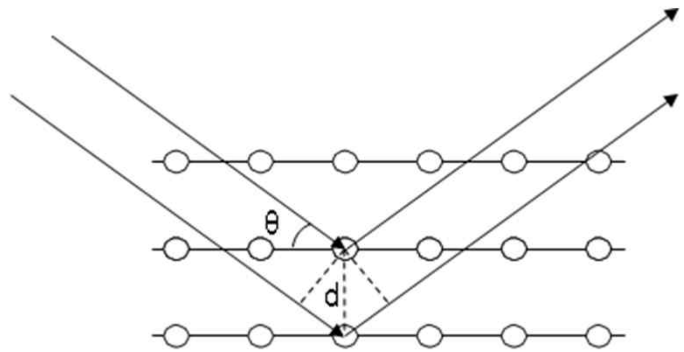

Crystal	2d	Energy Range
α-quartz (5052)	1.624	8.0 – 88 keV
Silicon (311)	3.274	4.0 – 44 keV
Silicon (220)	3.84	3.4 – 37 keV
Diamond (111)	4.118	3.2 – 35 keV
Silicon (111)	6.2712	2.1 – 23 keV
InSb (111)	7.4806	1.7 – 19 keV
Beryl (1010)	15.954	0.82 – 9 keV

Source: ALS/CXRO X-ray Data Booklet & XOP

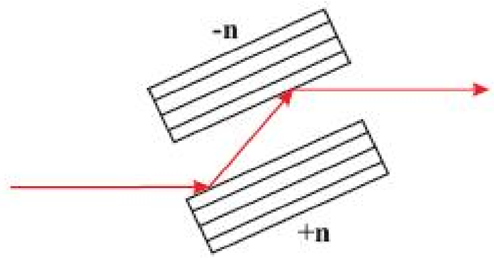

Double Crystal Monochromator

Double Crystal Monochromator

미래기반 가속기
전문인력양성 사업단

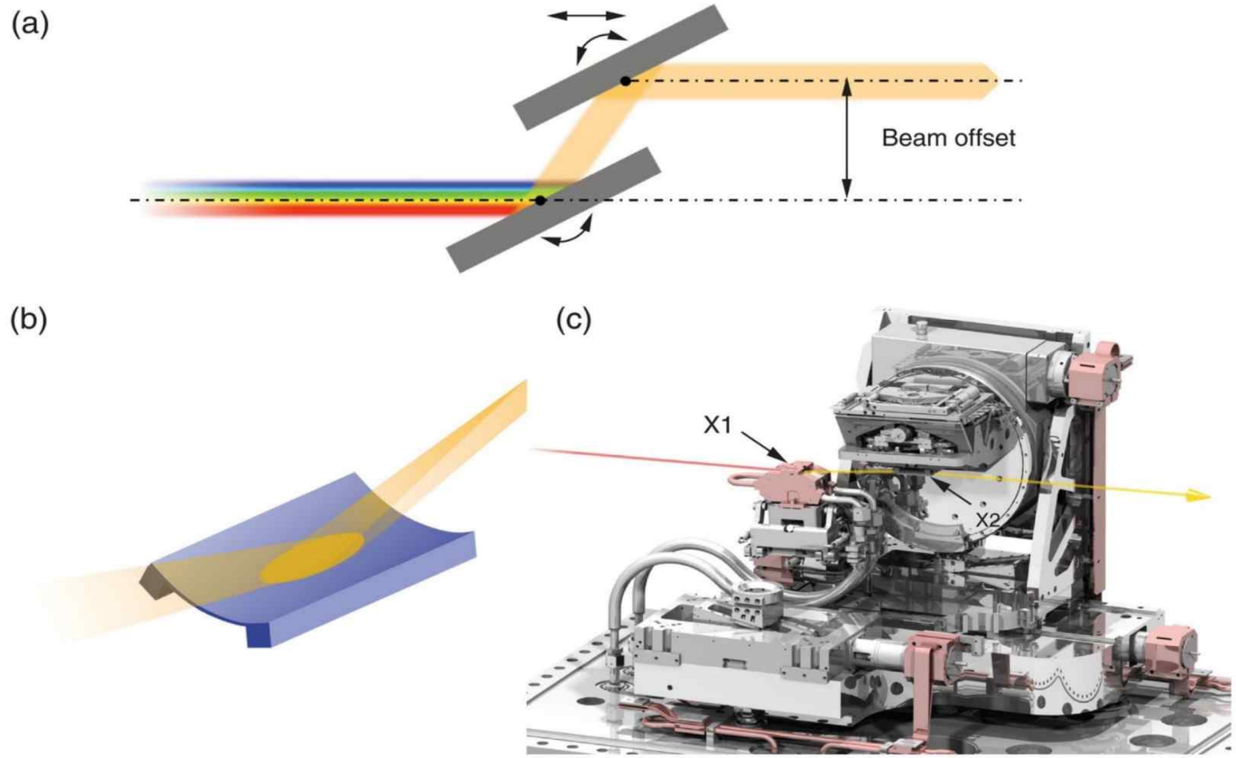

Figure 5.27 Double-crystal monochromators. (a) The geometry of a DCM. The first crystal monochromatizes the incoming polychromatic light, while the second crystal redirects the monochromatized beam parallel to the incoming beam. In order to keep the offset between the incoming and exit beam height constant for all photon energies (and monochromator crystal angles), the horizontal separation between the two crystals must be variable. (b) The second crystal can be dynamically flexed to 'sagittally' focus the beam in the horizontal plane. The bending radius of the crystal depends on the angle of incidence (in other words, the Bragg angle θ) and the desired focal position, and can be calculated using Equation (5.11). (c) A technical rendition of the DCM at the Materials Science beamline, Swiss Light Source. The path is shown of the incident polychromatic beam (shown in red) on the first crystal (X1) and the monochromated beam (in yellow) incident and diffracted off the second crystal (X2).

An Introduction to Synchrotron Radiation: Techniques and Applications, Second Edition. Philip Willmott.

WILEY

Effect of Heat Load on Monochromator First Crystal

Thermal gradient = “Thermal Bump”

undulator beam shows
a 0.3 micron bump.

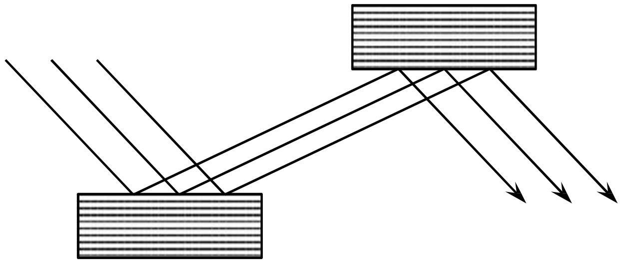

No heating of first crystal

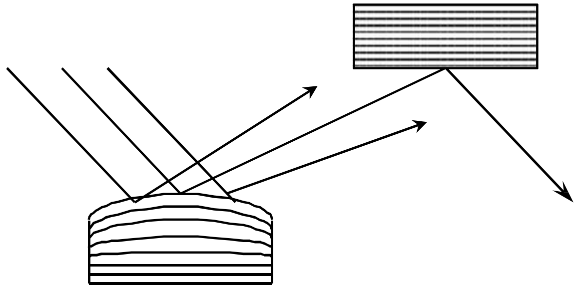

Heat “bump” on first crystal

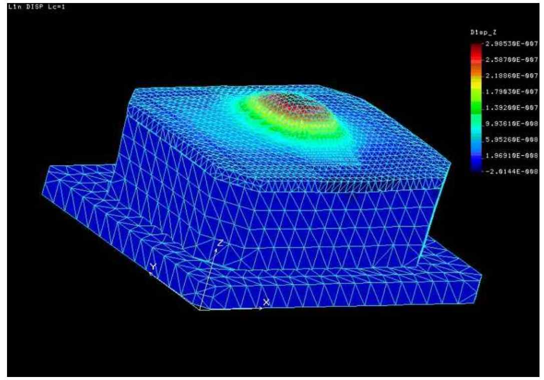

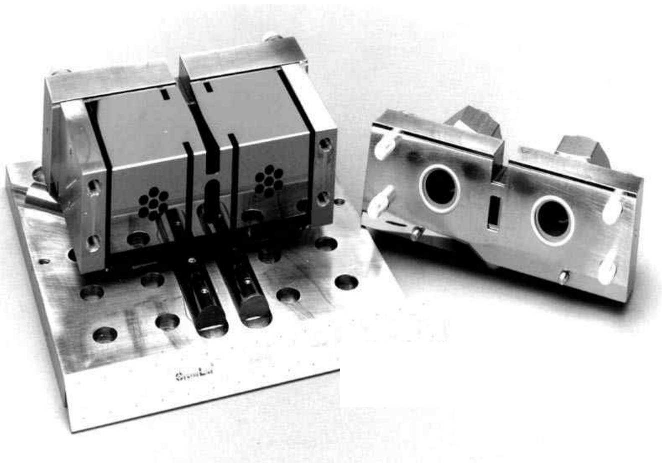

Liquid Nitrogen Cooled Silicon

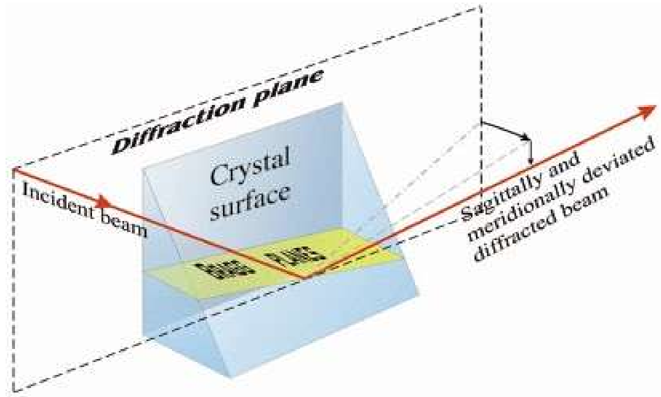

“Inclined Geometry” Crystal

Double Crystal Monochromator (DCM): Energy selection(10C XAFS BL,PLS-II)

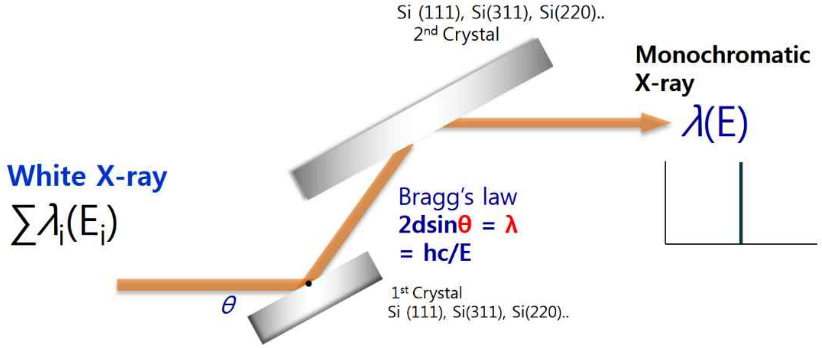

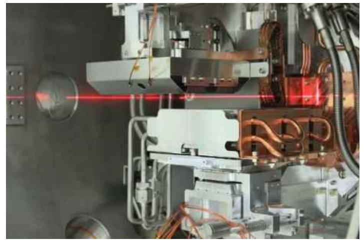

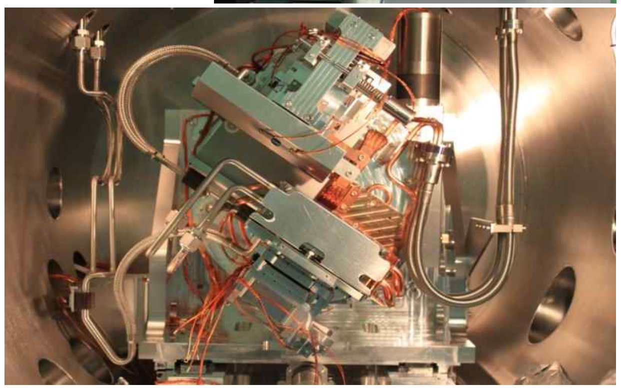

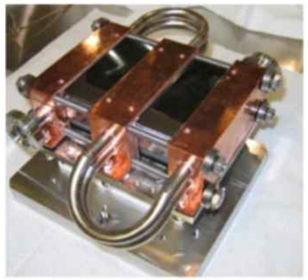

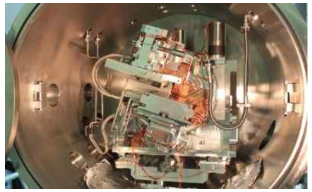

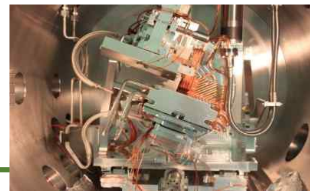

Dr. MGKim

Multilayer

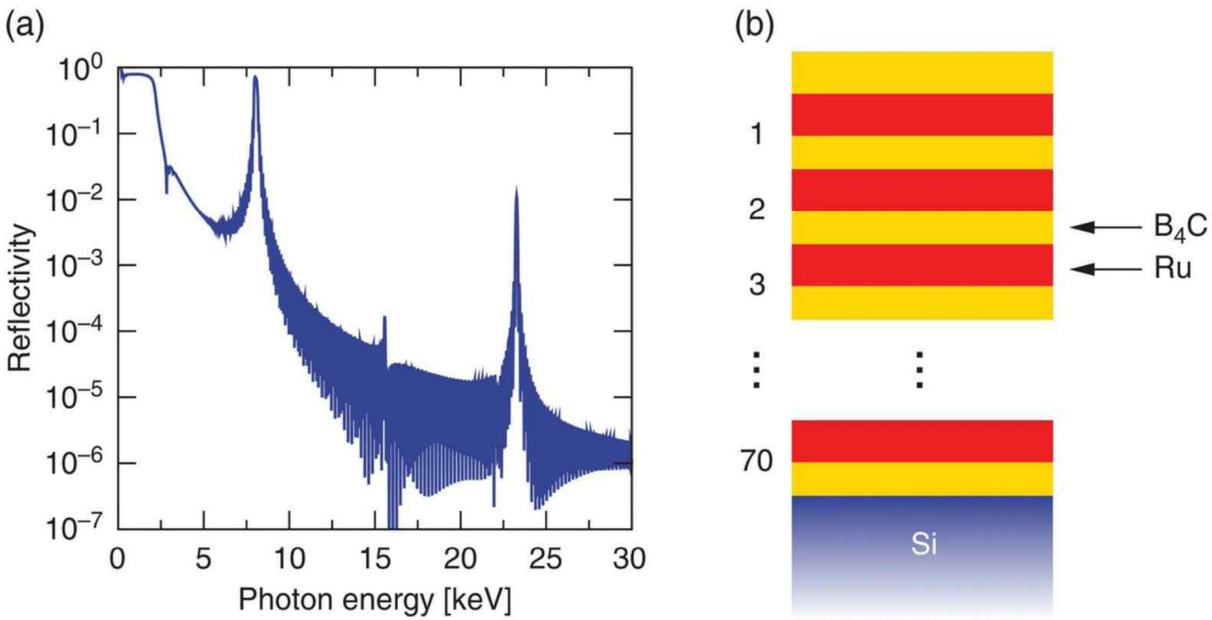

Figure 5.31 Multilayers used in monochromators. (a) The simulated reflectivity curve at an incident angle of 1.15° as a function of photon energy for the Ru/B_4C multilayer fabricated for the BM5 beamline at the ESRF. (b) A schematic of the structure [12].

An Introduction to Synchrotron Radiation: Techniques and Applications, Second Edition. Philip Willmott.

WILEY

Three Common Grating

Figure 5.21 Three common grating profiles used to disperse ultraviolet light and soft x-rays.

An Introduction to Synchrotron Radiation: Techniques and Applications, Second Edition. Philip Willmott.

WILEY

Diffraction Gratings

✓ **The grating equation.**

$$d(\sin\beta - \sin\alpha) = m\lambda$$

d = grating line spacing

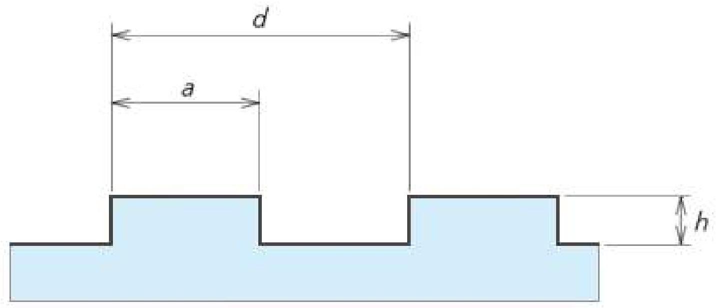

Groove depth : *h*
Duty ratio : *a/d*

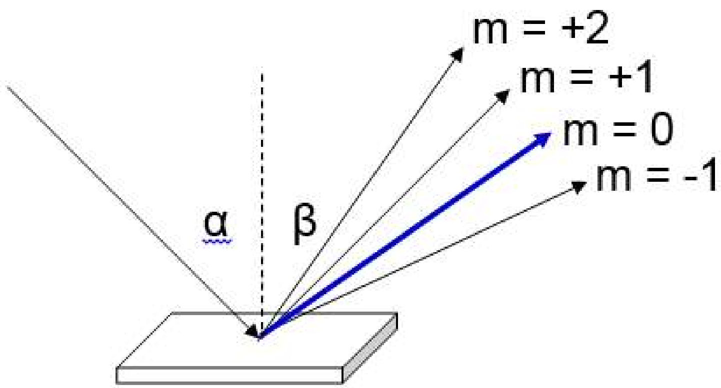

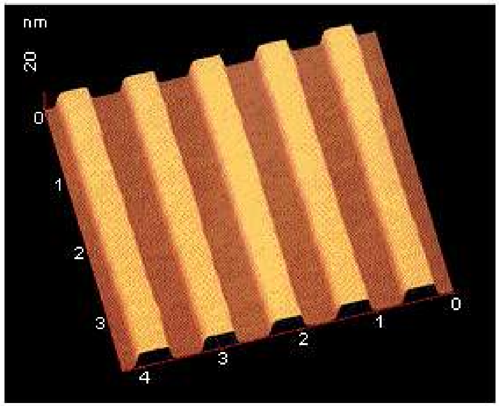

- Diffraction gratings are used from visible (and beyond) to soft X-ray energies. Gratings can function up to and above 2 keV, with decreasing efficiency
- Practical limit on line spacing is about 2000 lines/mm
- Most monochromators use first order diffraction
- Most gratings are "blazed", ie the groove profile is figured to optimize for certain angle/wavelength ranges.

- Unlike crystal diffraction, all energies are diffracted all the time. An exit slit is needed to select a monochromatic beam.
- Zero order is not dispersed (grating acts like a mirror, ie α = β).

Grating's groove depth, width and photon energy

미래기반 가속기
전문인력양성 사업단

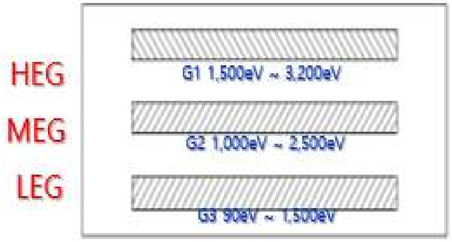

	Density[mm-1]	Groove depth[mm]	Photon Energy Range[eV]	IA[°]
HEG	1500±1%	9±3 nm	1,500 ~ 3,200	177.2
MEG	600±1%	12±4 nm	1,000 ~ 2,500	176
LEG	400±1%	16±4 nm	90 ~ 1,500	172

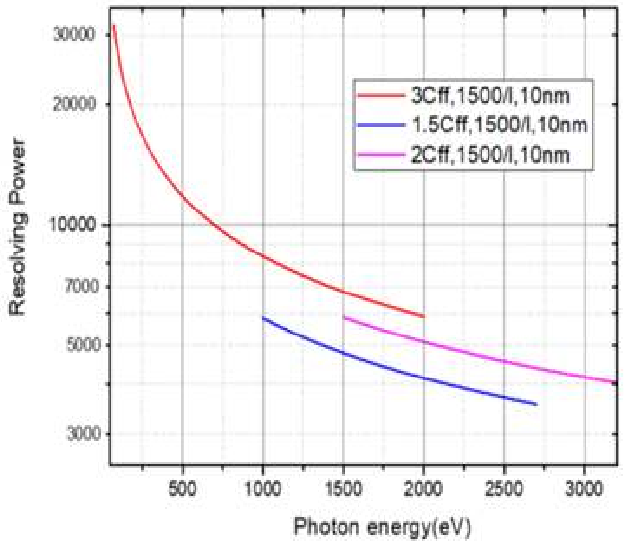

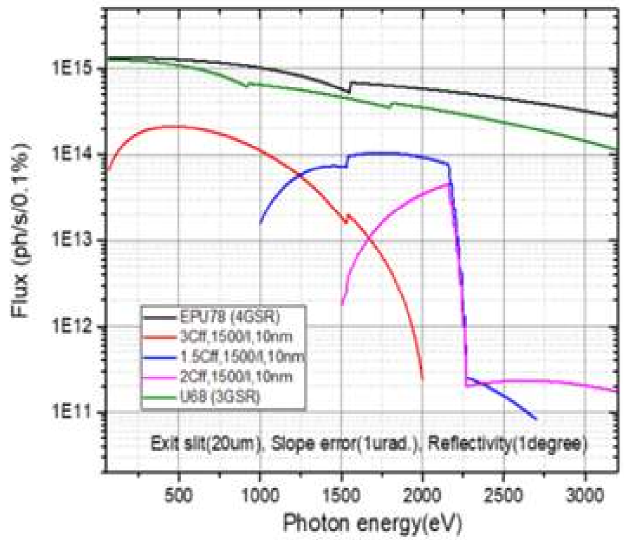

Beamline Design Goals

- **Deliver the required X-ray beam to the experiment:**
  - ✓ Energy and bandwidth
  - ✓ Spot size
  - ✓ Divergence/convergence
- **Preserve source characteristics eg intensity, brightness, coherence**
- **Handle the heat load of the beam**
- **Optimize signal / background**
- **Be very stable and reproducible, in position, intensity and energy**
- **Be safe to operate**
- **Be user friendly to operate**
- **Achieve all the above within a reasonable budget !**

Layout of Soft X-ray Beamlines(8A)

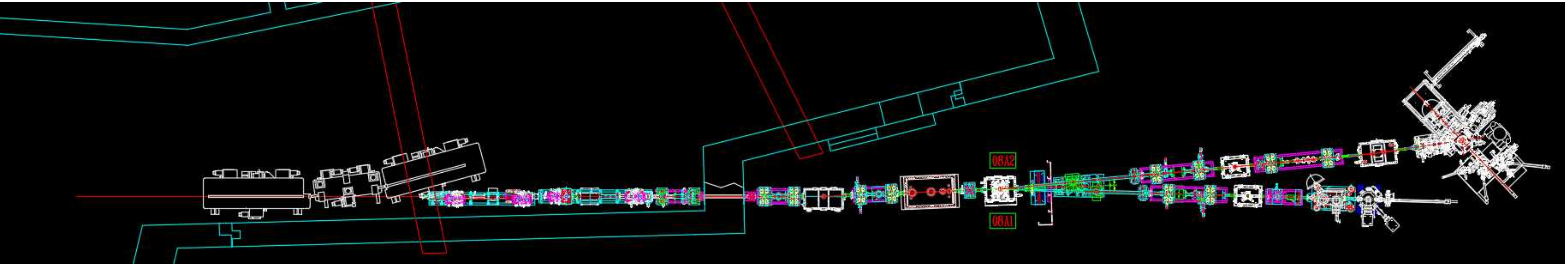

- Photon Source : Undulator (Out vacuum undulator)
- Vacuum system
- Optical system : Mirror, Plane Grating Monochromator,
- Beam diagnostic system
- Slit
- Experimental system
- Utilities
- DAQ,
- Electrical system
- Interlock system
- Safety : Radiation Safety, Gas safety, Laser safety
- …….

Courtesy of YDYoun

Layout of hard X-ray Beamlines(3C)

미래기반 가속기
전문인력양성 사업단

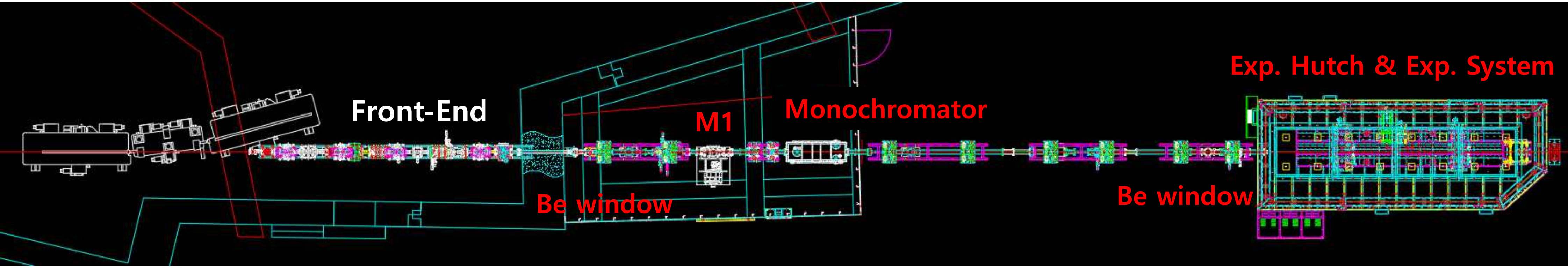

- Photon Source : Undulator (in-vacuum)
- Vacuum system
- Optical system : Mirror, Double Crystal Monochromator,
- Beam diagnostic system
- Slit
- Experimental system(inside Hutch)
- Utilities
- DAQ,
- Electrical system
- Interlock system
- Safety : Radiation Safety, Gas safety, Laser safety
- ....

Example) What we did to construct 8A Beamline

Pronounced the anion site relatively.

미래기반 가속기
전문인력양성 사업단

Cation

10A1 STXM

Keyword for Required Beamline
: High Photon Flux
: Cover Wide range of photo

8A1 SPEM

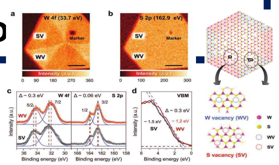

Advanced Materials (2017)

8A2 APXPS

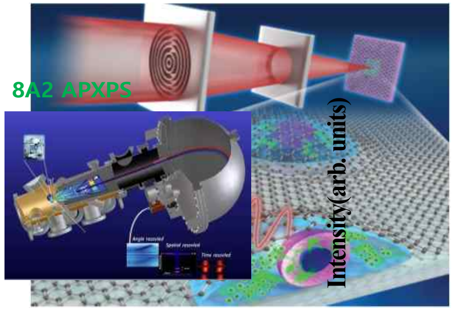

Nanoscale(2018)

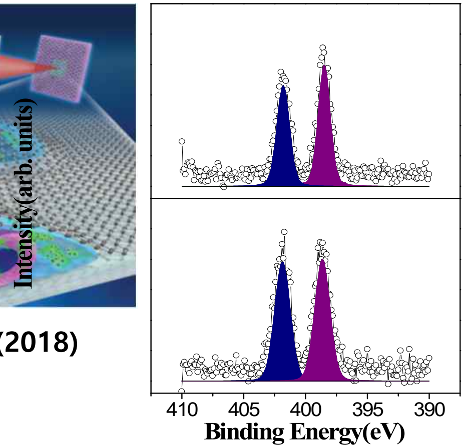

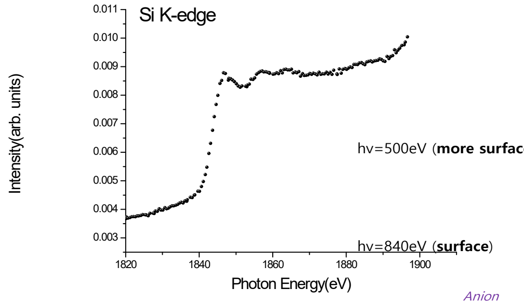

Anion

- **10A beamline branching**
  - Keep 10A1 STXM as it is.
  - Accept 8A2 HR-PES II user.
  - → **10A1 STXM/10A2 HR-PES II**
- **8A beamline reconstruction**
  - Photon energy : 200 ~ 2000eV(Practical)
    (100 eV ~ 3000eV, available)
  - Photon Flux : ~ > 10^{13}
  - Beam size : < 50μm
  - Resolving power : > 4000 ~ 10000
  - → **8A1 SPEM/8A2 KBSI – PAL APXPS**

Resources for 8A Beamline

Electron Beam

Parameter	Value
Beam energy	3 GeV
Beam current	200~400mA (Max. 400 mA)
Lattice structure	Double-Bend
Super-period	12
Emittance	5.8 nmrad
Tune (H/V)	15.375/9.145
RF frequency	499.96 MHz
Energy spread	0.1 %

Major Parameter for PLS II

Photon Source :Undulator

Deflection parameter K

$$K = \frac{eB_0\lambda_u}{2\pi m_e c}$$

$$E = \frac{2n\gamma^2 hc}{\lambda_u\left(1 + \frac{K^2}{2} + \theta^2\gamma^2\right)}$$

Device total length : 3.3 m
Periodic length(λ_u) : 6.8 cm

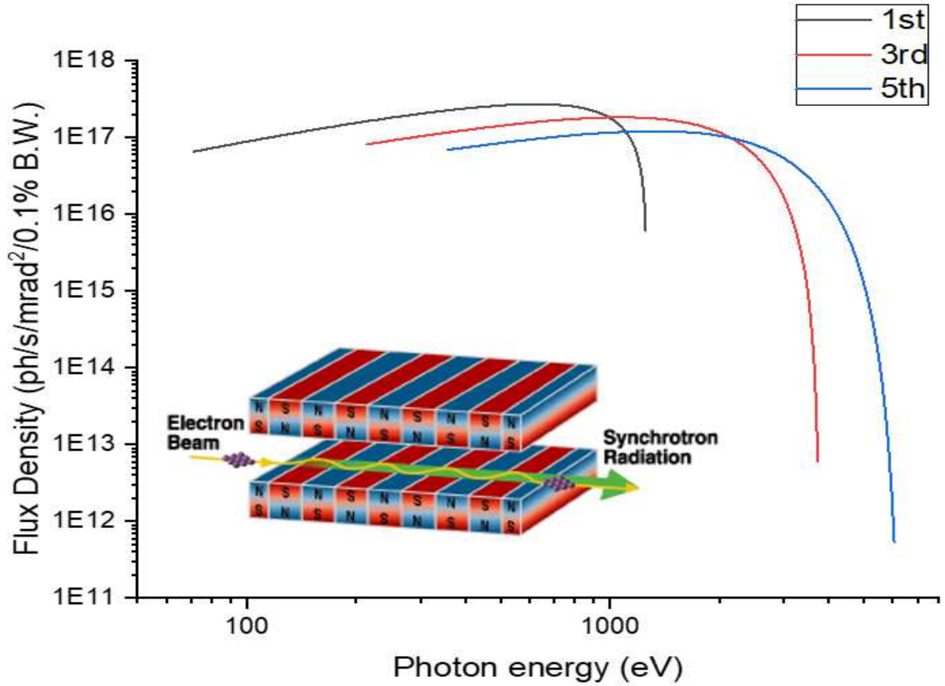

Beam size at Mirrors

Beam shape at M1 mirror

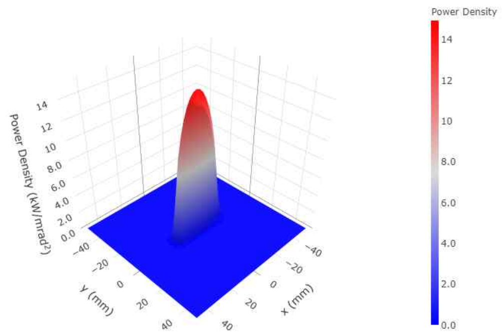

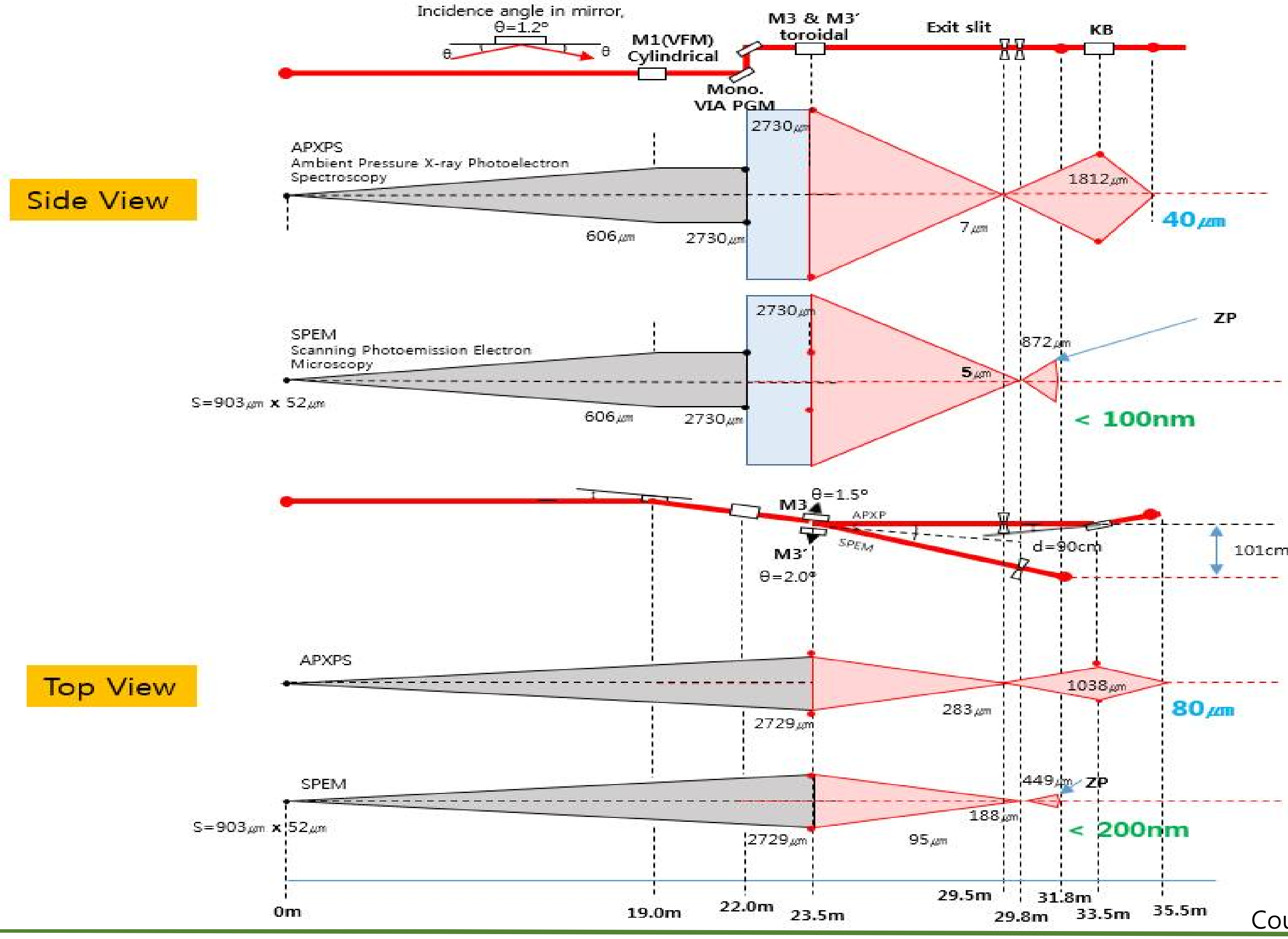

Courtesy of JYBack

Mirrors spec.

Shadow

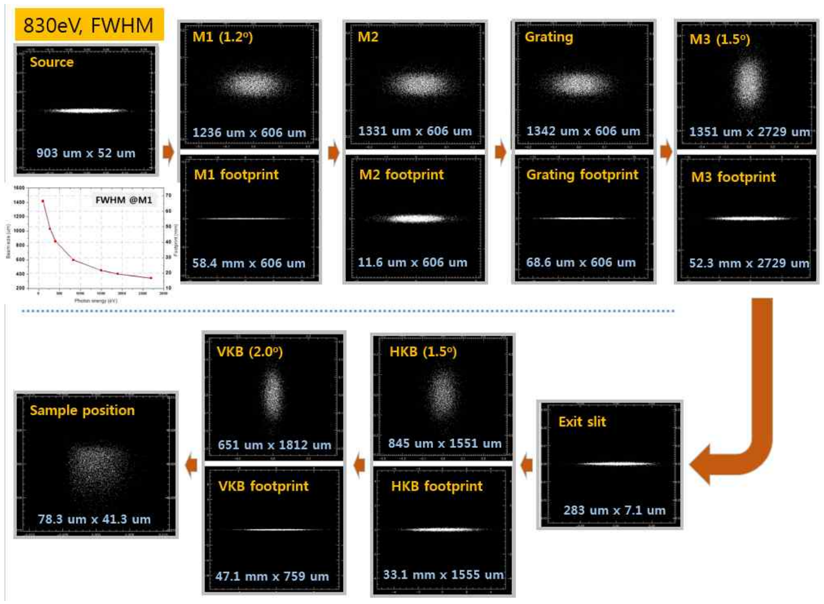

	M1	pre-	Grating	M3(8A2)	M3'(8A1)	HKB	VKB
Max. size@mirror(fp)	79.1	24.7	46.7	76.3	76.3	33.6	116.9
Incident Angle	88.8	86~88.6	86.45~89.09	88.5	88	88.5	88
Max. Beam size(H)	1.67	1.87	1.91	1.65		0.91	0.67
Max. beam size(V)	1.53	1.42	1.42	6.34		3.5	3.96
Clear Aperture	140	110		112		66	196
Mirror Size(L x W)	200 x 40 x 50	380 x 80 x 50	(80x10) x 4 x 20	160 x 50 x 50		120 x 50 x 50	240 x 50 x 50
Cooling	Internal	Internal	In-Ga				
Function	Cylindrical V-collim.	plane	plane	Toroidal	Toroidal	Cylindrical H-focus.	Cylindrical V-focus.
Tangential®	infinite	infinite	infinite	400000	320000	108800	75500
sagittal®	8012.3	infinite	infinite	3138	4400		

Monochromator(VIA-PGM)

Needed photon specs. (cover 200~2,700 eV, >~10^{12} photons/sec)

❖ **Variable inclusive angle for covering wide photon-energy range.**

- IA′ = 180 – IA (inclusive angle)
- **Angle accuracy: < 10^{-5} °**

	DMG (mm)	D (mm)	IA' (°)	α (°)
Min.	85.069	15	10	86
Max	357.889	15	2.4	89.5

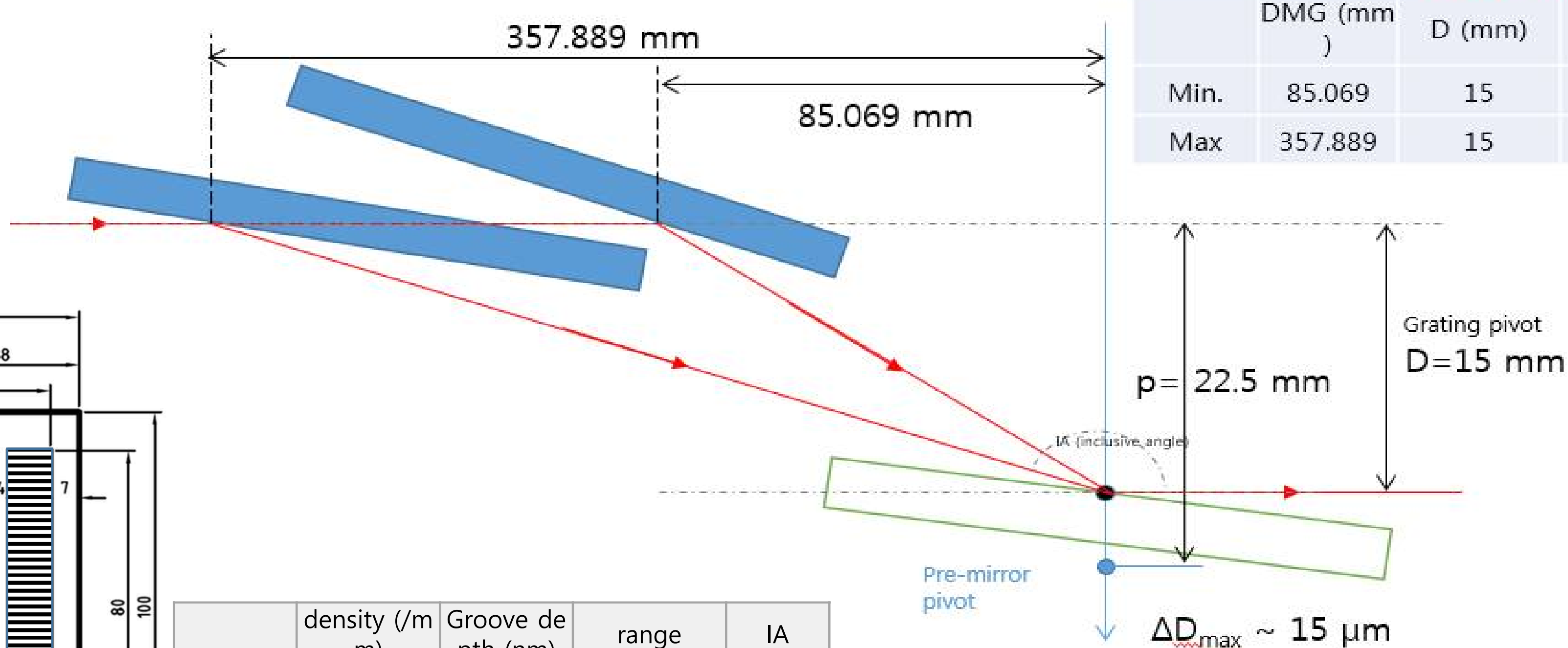

Beam size at grating at 89 ° : ~40 mm (4σ)

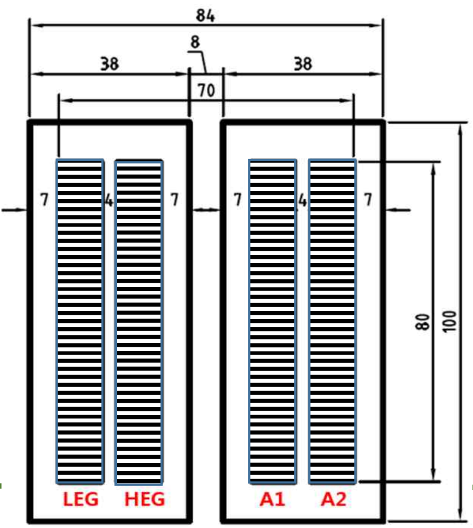

	density (/mm)	Groove depth (nm)	range	IA
LEG: G2	400	16	250-900	175
HEG: G4	600	9	700-2000	176
A1	350	22	100-400	172
A2	500	8	1200-3000	177.2

Courtesy of JYBack

Monochromator, Resolving powers (ray-tracing)

❖ Total resolving power: main: 5,000~18,000, aux: 3,000~25,000

$c = \cos\beta/\cos\alpha$: focus constant

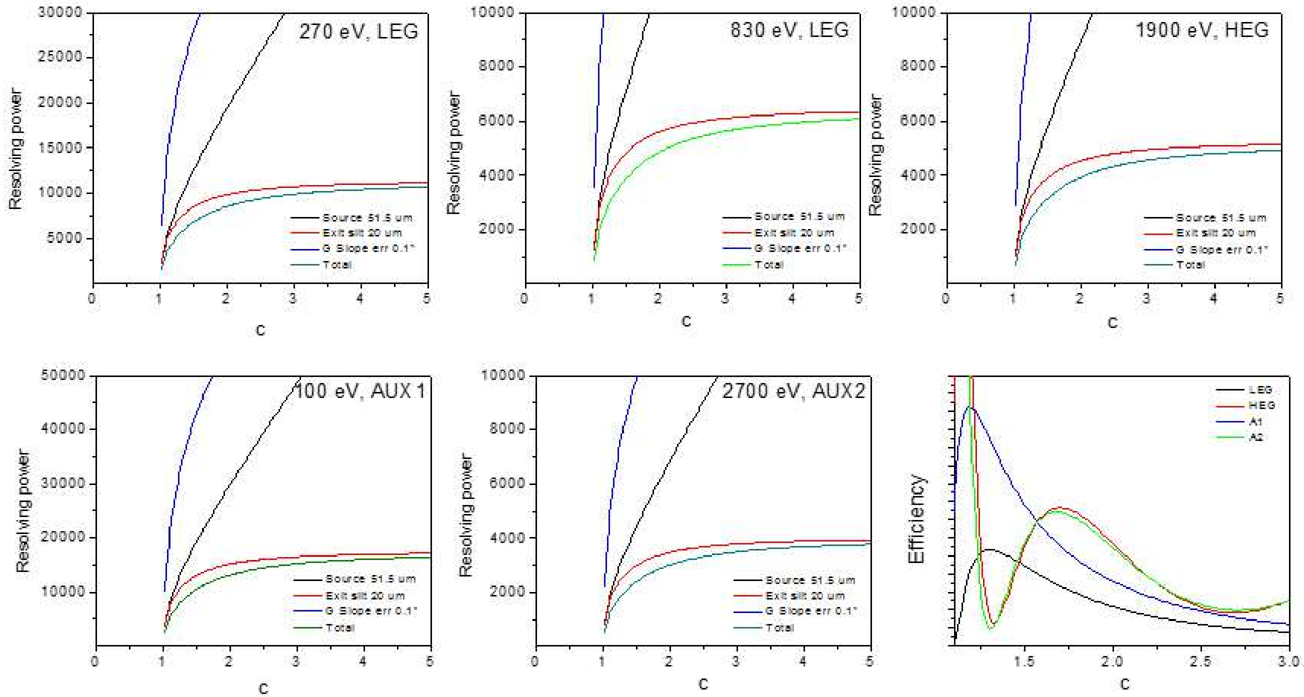

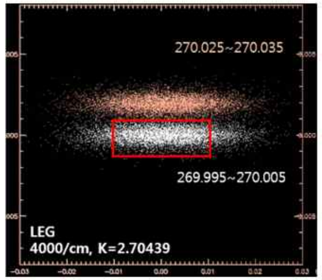

LEG : R.P ~ 9000 @ 270eV

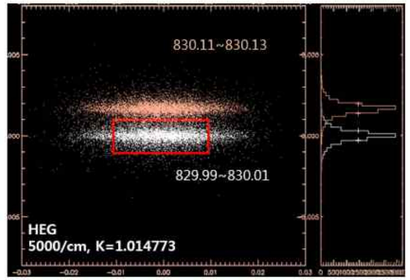

HEG : R.P ~ 7000 @ 830eV

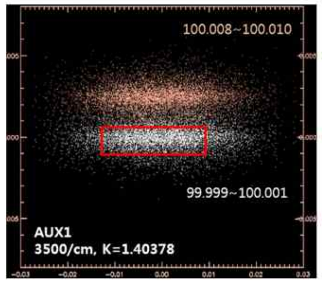

AUX1 : R.P ~ 11000 @ 100eV

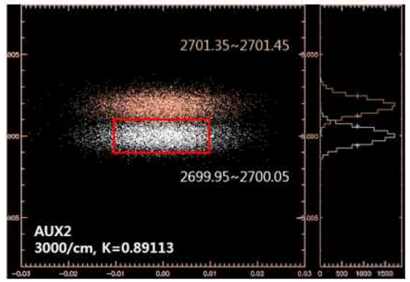

AUX2 : R.P ~ 2000 @ 2700eV

❖ ΔE 1: entrance spread, ΔE 2: Exit width spread., ΔE 3: G slope Err. ΔE Tot: S.R. sum
❖ Source width: 51.5 um, Exit slit: 20 um, Slop error: 0.1” (0.485 urad), D(StoSlit)=19, D(GtoExS)=7.5

8A1 SPEM
8A2 APXPS

Since May 2019

미래기반 가속기
전문인력양성 사업단

Goal for Optical design

: Photon Energy range : 100 ~ 2000eV (practical range)

: Resolving power : 9000 (< 700eV), 3000 (> 700eV),
Photon flux : ~ 10^{13} (photon/sec/0.1%B.W.)
Beam size : 40 um x 80 um @ APXPS, 100 nm x 200 nm @SPEM

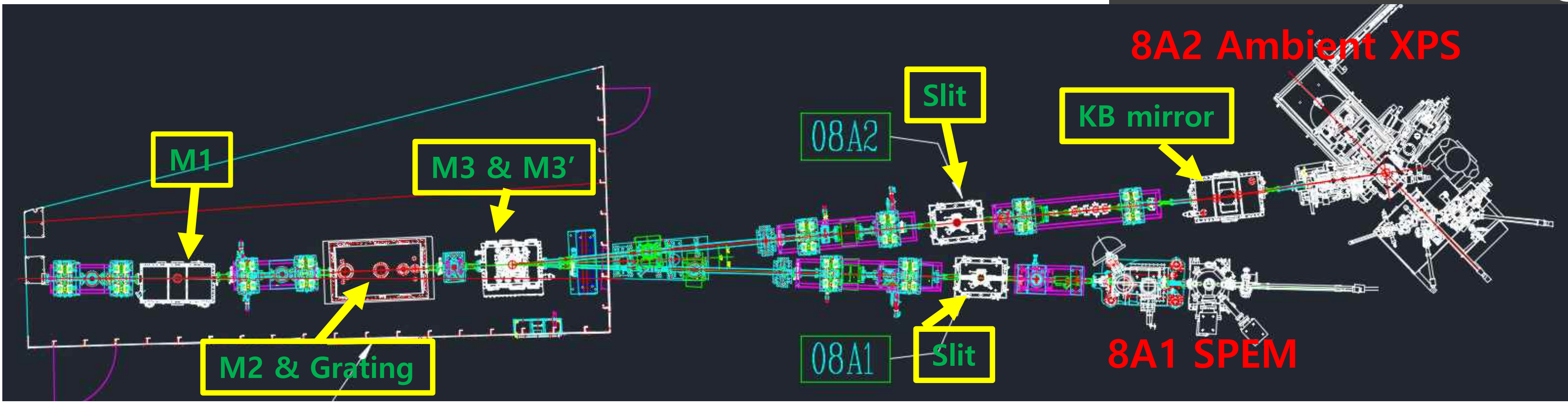

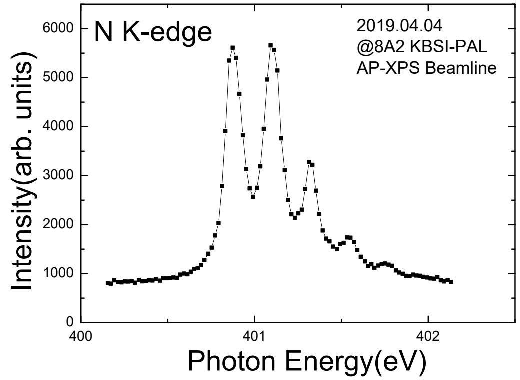

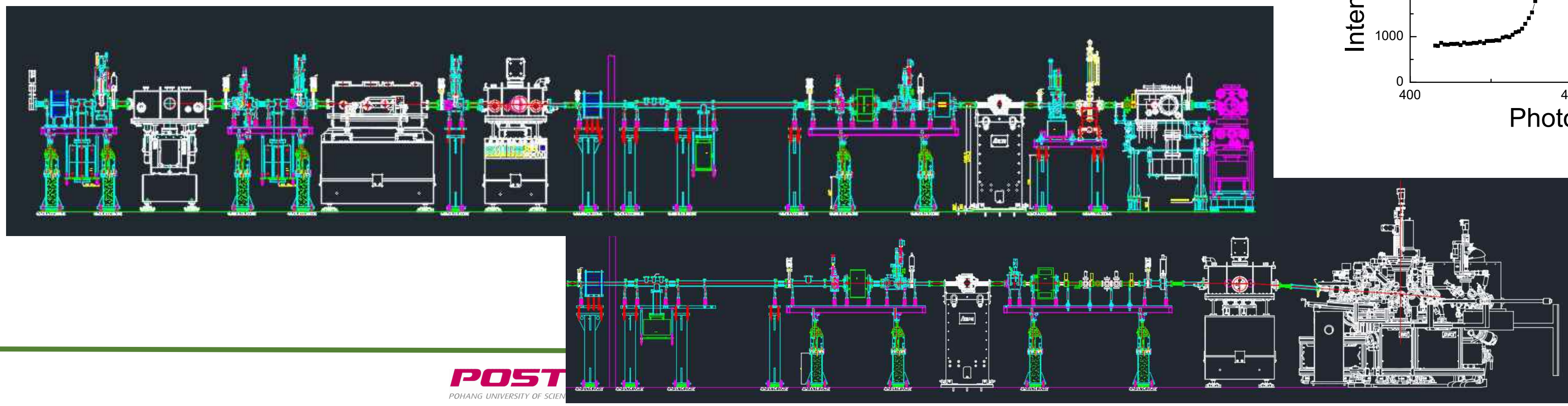

Exp. Floor View

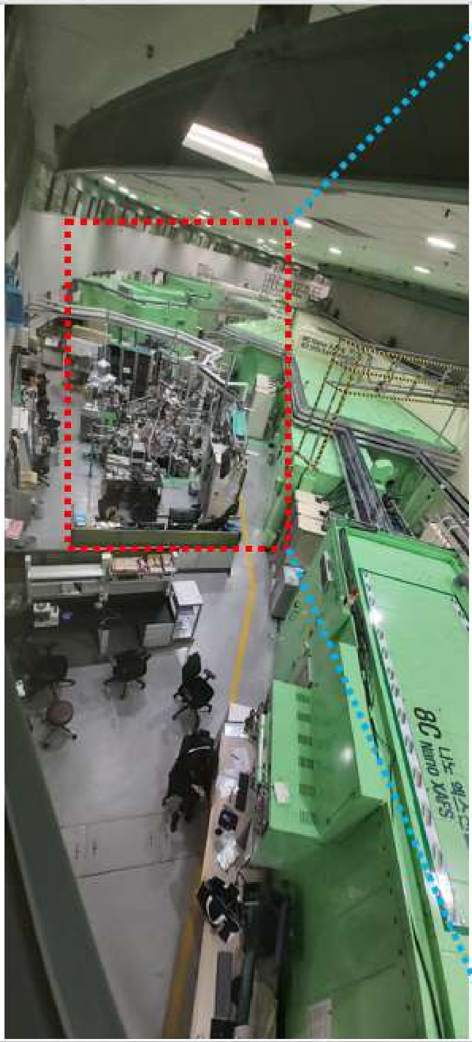

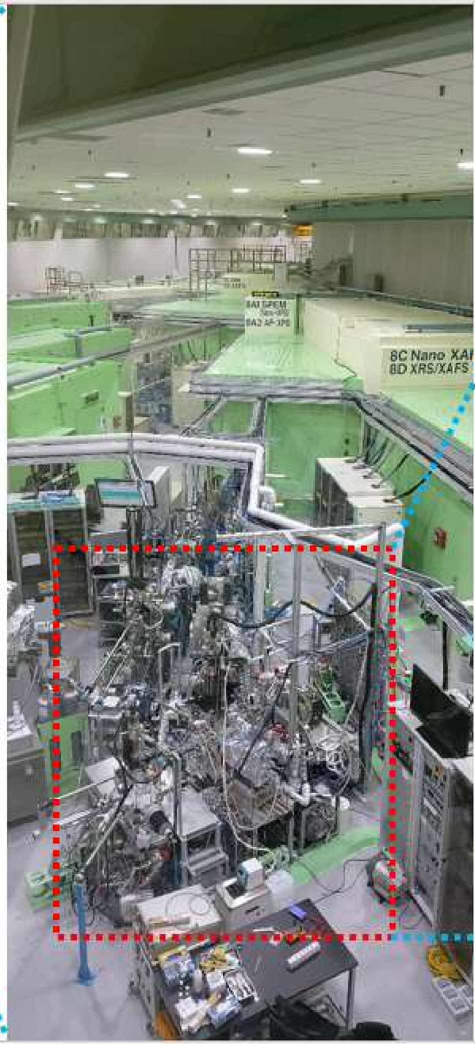

Cell #8 : Exp. Floor View

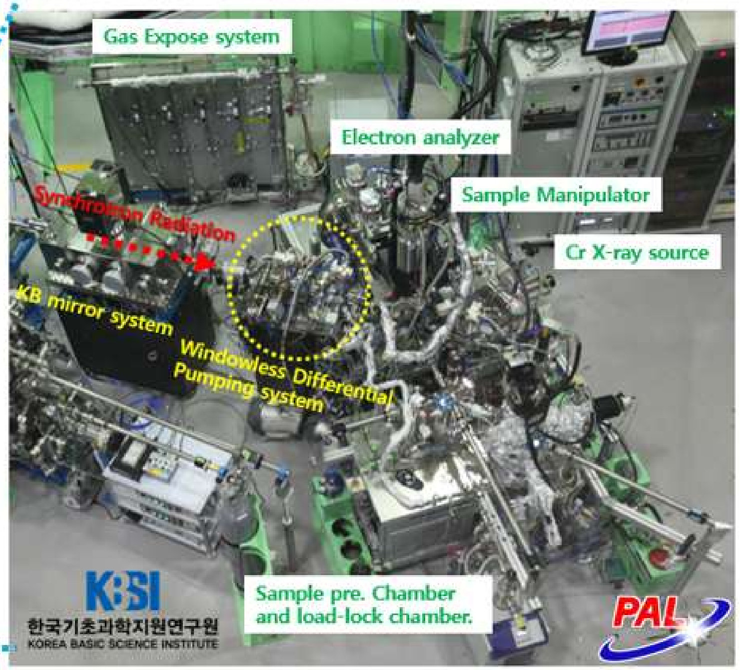

Research Opportunities using Synchrotron Radiation

PLS-II Beamline Map

포항가속기연구소 과학기술정보통신부

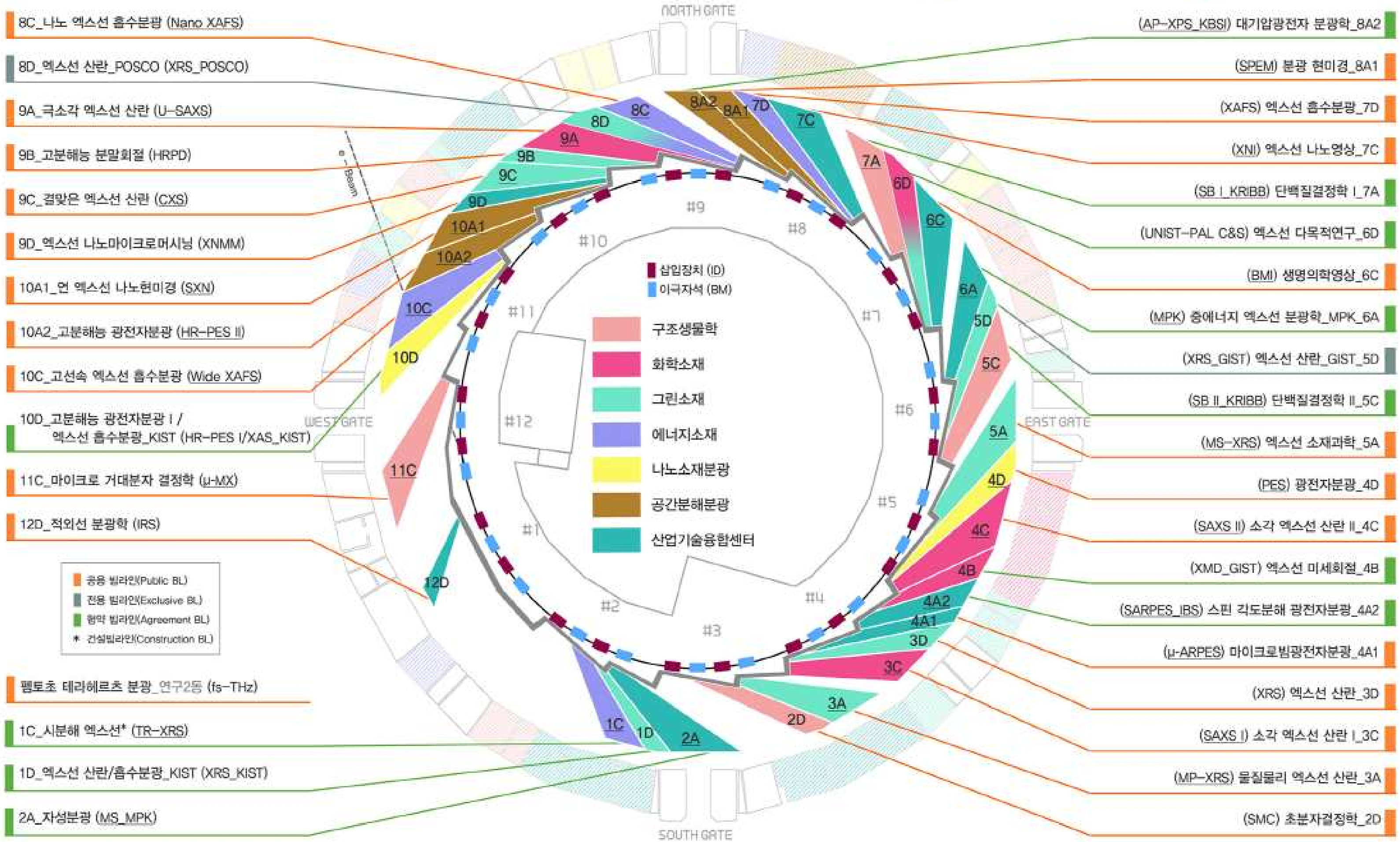

Versatile Sample Systems

미래기반 가속기
전문인력양성 사업단

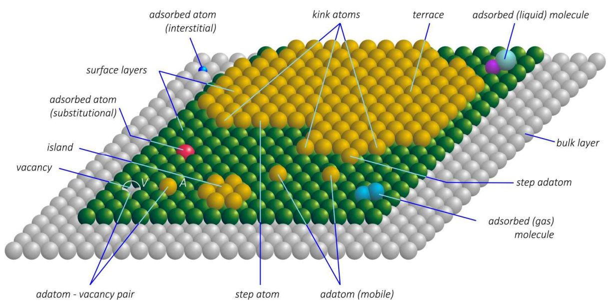

https://en.wikipedia.org/wiki/Terrace_ledge_kink_model#/media/File:Crystal_surface.jpg

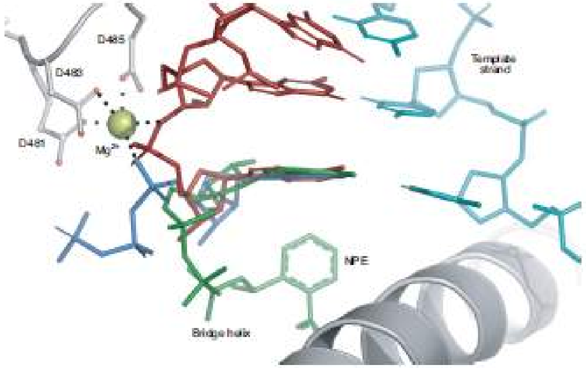

Nature Methods 18, 431(2021)

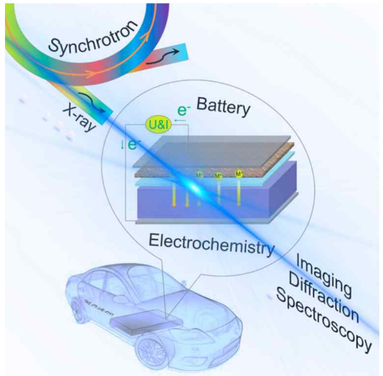

Chem. Rev. 117, 13123−13186(2017)

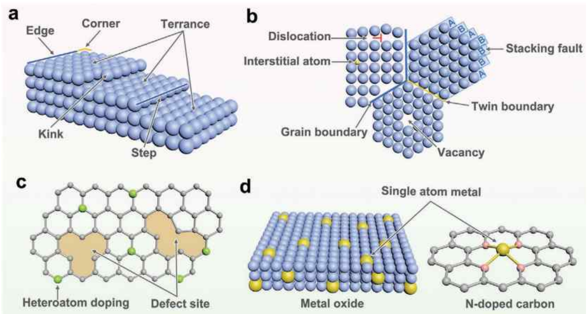

Adv. Mater. 2020, 32, 2002435

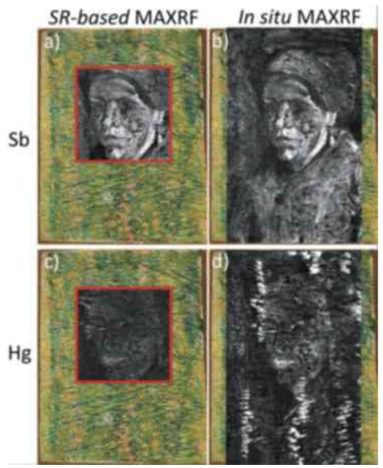

IAEA-TECDOC-1803

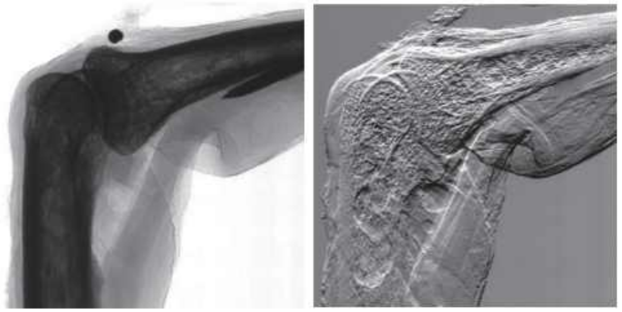

Phil. Trans. R. Soc. A 377: 20180240.

Detectors

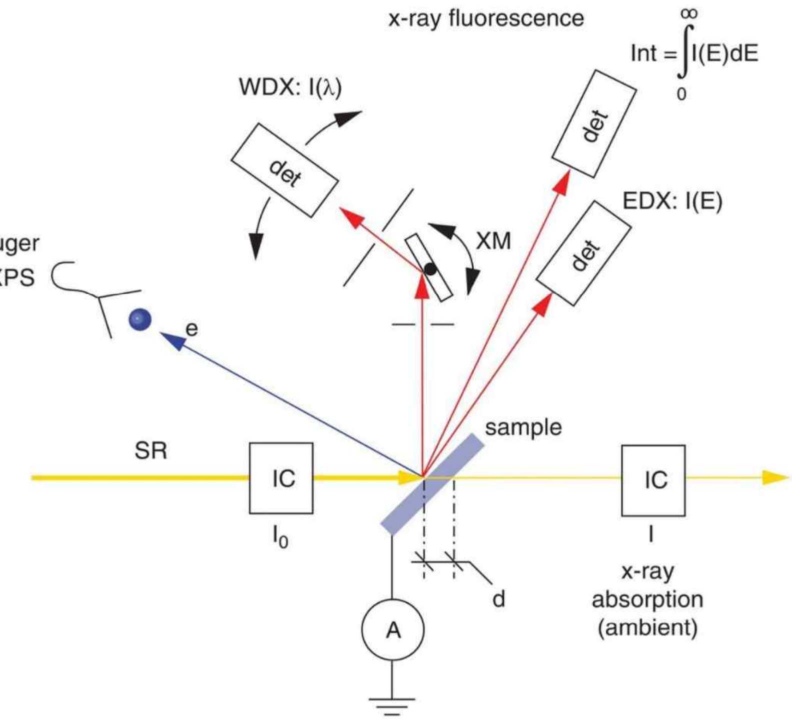

Figure 7.3 X-ray absorption and x-ray fluorescence experiments. Monochromatic synchrotron radiation (SR) is allowed to impinge on a sample. X-ray absorption spectra can be recorded by measuring the amount of light that passes through a thin sample. The x-ray intensities before entering the sample (I_0) and after (I) are measured using ionization chambers (IC), or other beam-intensity monitors, and is particularly suited for samples that cannot be placed in vacuum, such as in biological or catalytic experiments. The total electron current (A) can also be used to indirectly determine the absorption spectrum. In this case, the sample and detectors must be in vacuum. X-ray fluorescence spectra can be recorded, either using a crystal monochromator (XM) in wavelength-dispersive spectra (WDX), or by using a dispersive solid-state semiconductor device (EDX). The integrated fluorescence yield can also be used as a measure of absorption strength. Unwanted detection of elastically scattered x-rays is best achieved by placing the detector on the polarization axis of the synchrotron radiation (see also Figure 2.8).

An Introduction to Synchrotron Radiation: Techniques and Applications, Second Edition. Philip Willmott.

WILEY

How to prepare a sample surface?

-Ex. Situ. Sample

Sample Transfer to Vacuum Chamber

Analysis as it is

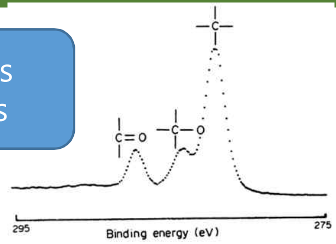

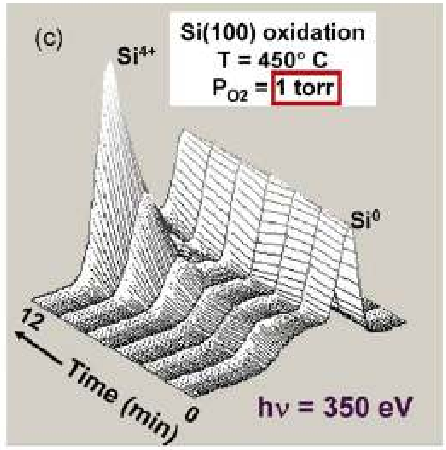

-In Situ. Sample

Sample Transfer to Vacuum Chamber

Analysis

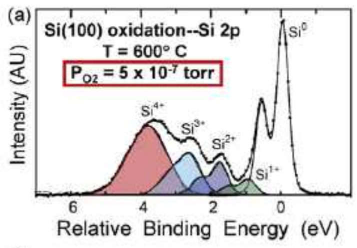

Sample Cleaning & Reconstruction

Annealing & Flashing

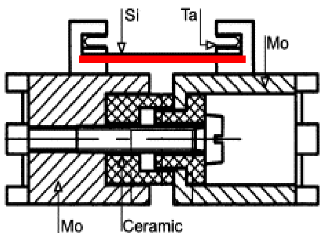

Cleaving

blade

Sputtering & annealing

ion beam

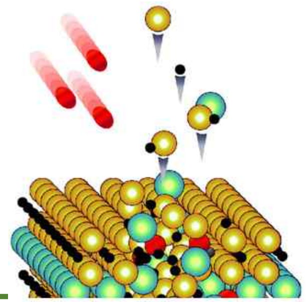

Evaporation

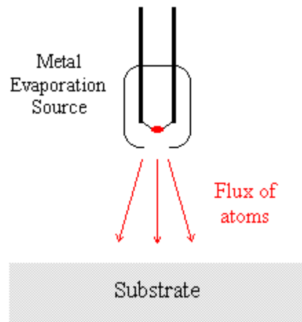

Surface Study

미래기반 가속기
전문인력양성 사업단

Exp. Beamline : 10A2

❖ Electron Escape Depth

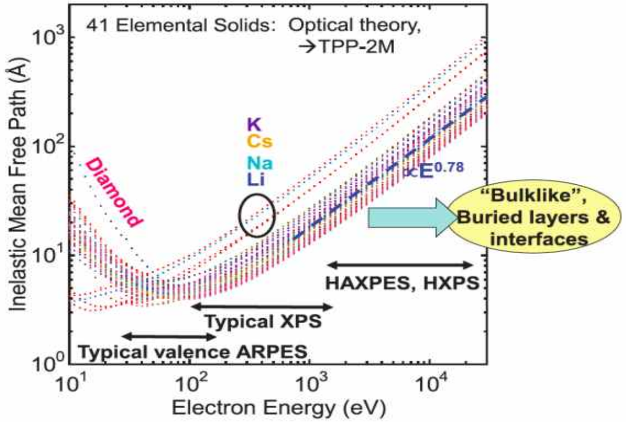

C. S. Fadley and S. Nemšák,
J. Electron Spectrosc. Relat. Phenom. 195, 409–422 (2014).

➢ Ring-Opening Reaction of Tetrahydrofuran on the Ge(100) Surface

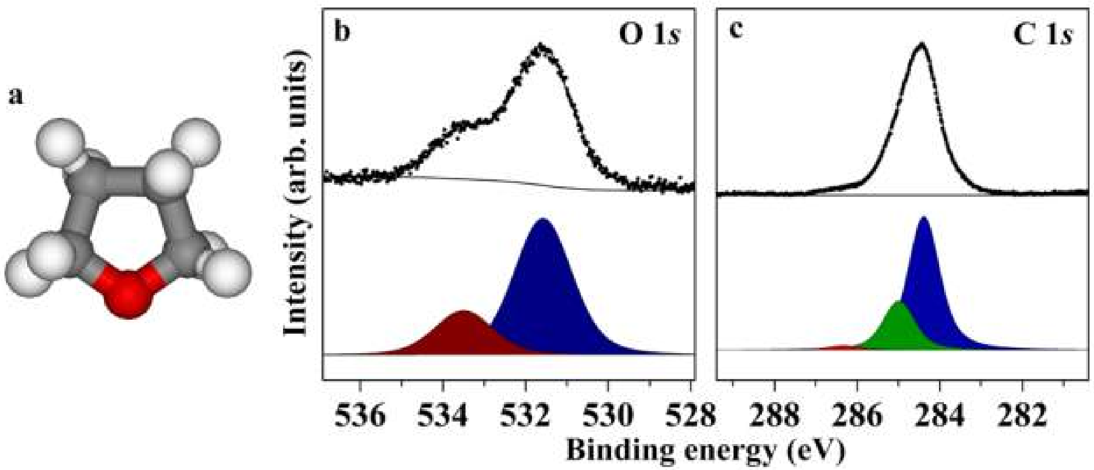

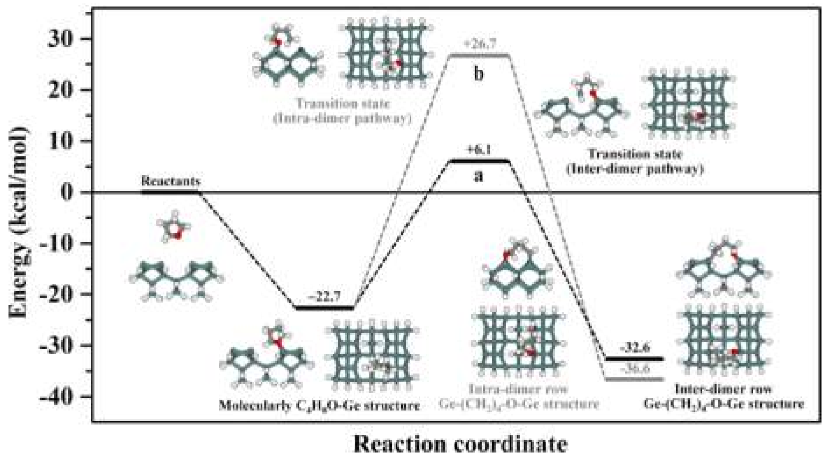

S. Park, et. al, ACS Omega accepted(2020)

Surface Study

미래기반 가속기
전문인력양성 사업단

Exp. Beamline : 8A2

➢ Nature of the surface space charge layer on undoped $SrTiO_3(001)$

- ABO_3-type perovskite structure
  Colossal magnetoresistance (CMR),
  Metal–insulator transition (MIT),
  High Tc superconductivity,
  Two- dimensional electron gas (2DEG)
- interfacial layers where different complex oxides form are mainly responsible for these exotic features

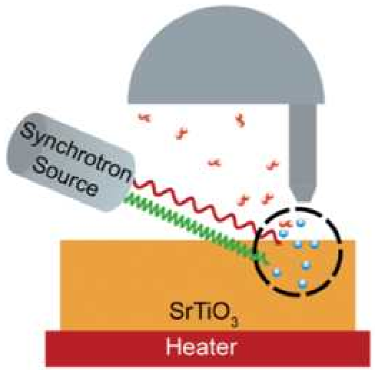

❖ Experimental scheme

❖ SrO_{1+x} surface oxide (orange)
❖ $SrTiO_3$ lattice oxide (cyan)

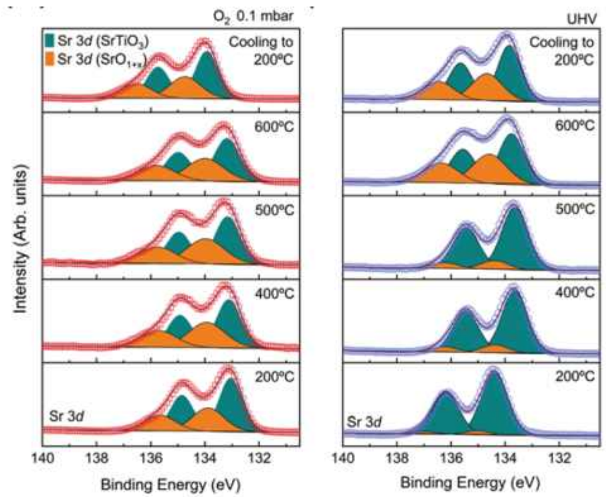

❖ Comparison of Sr 3d spectra at different probing depths

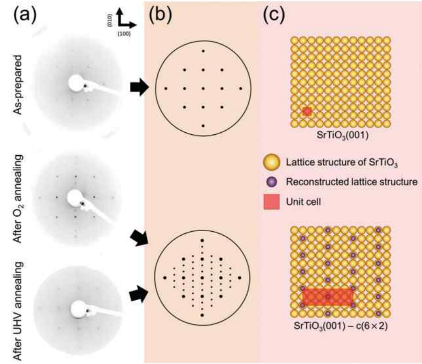

❖ Characteristic binding energy positions of the $SrTiO_3$ lattice component as a function of annealing temperature

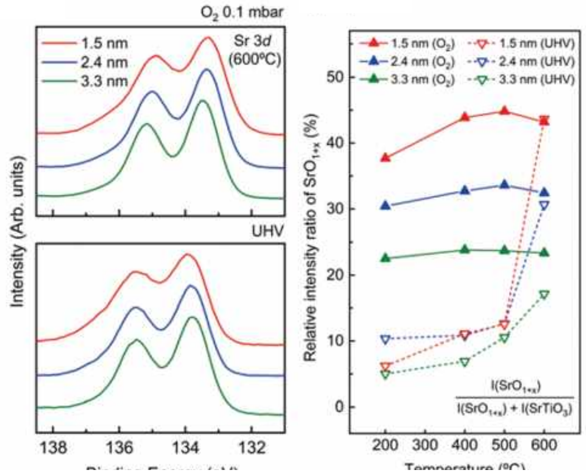

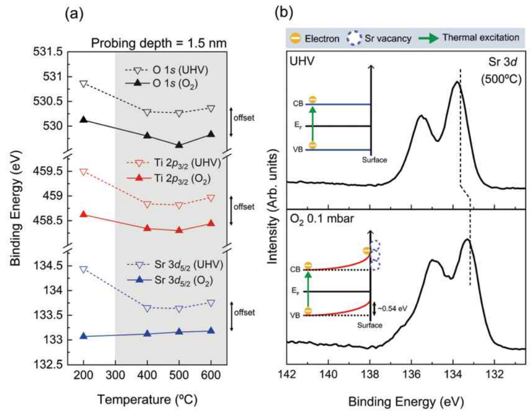

H. Lim et al, J. Mater. Chem. C DOI: 10.1039/d1tc03436g(2021)

Semiconductor Industry

❖ Nano-Scale Analysis Using Synchrotron-Radiation

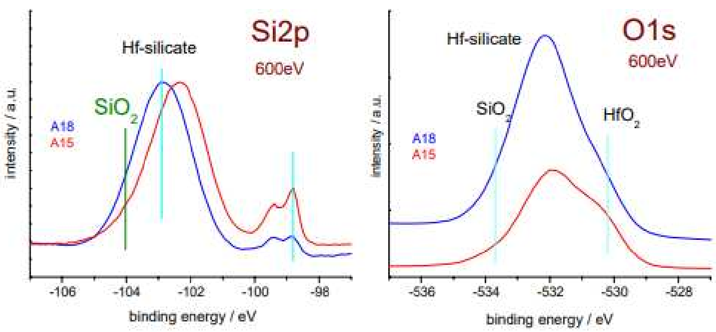

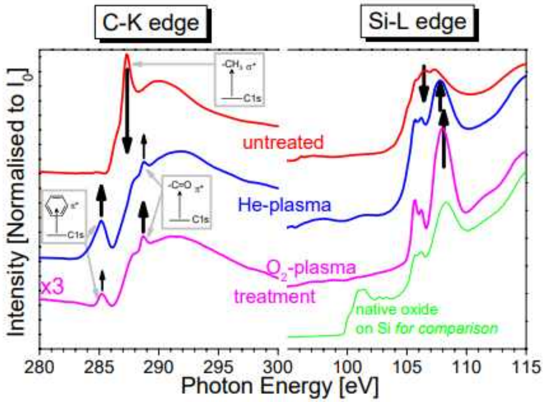

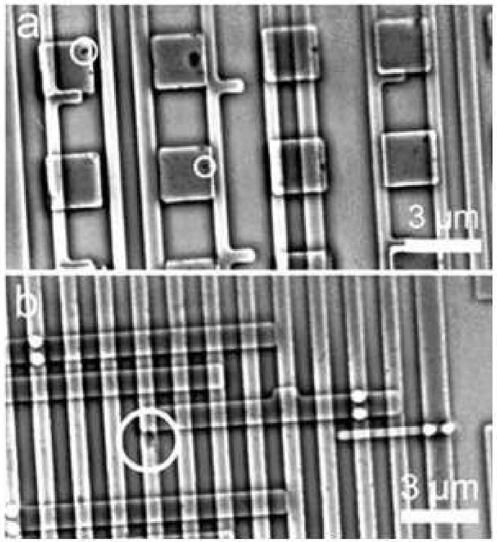

❖ Irregularities in the square structures: Several copper interconnect structures, imaged in positive phase contrast mode in the ID21 transmission X-ray microscope.

❖ EUV patterning

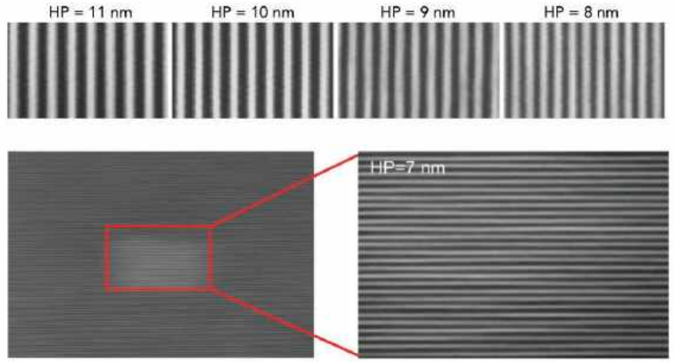

SYNCHROTRON RADIATION NEWS, 32,22(2019)

❖ EUV ring at PAL(under construction)

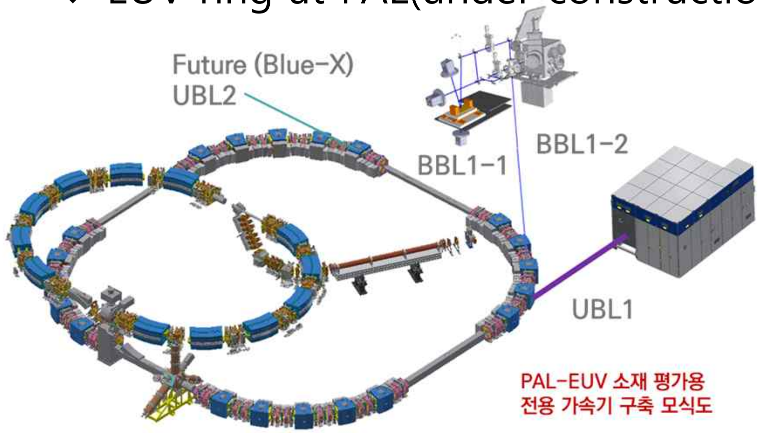

Current Nanoscience, 2008, Vol. 4, No. 3 259

Determination of Arsenic Poisoning and Metabolism in Hair

Elemental maps, obtained on Vincent van Gogh's "Patch of Grass", showing the hidden portrait of a woman.

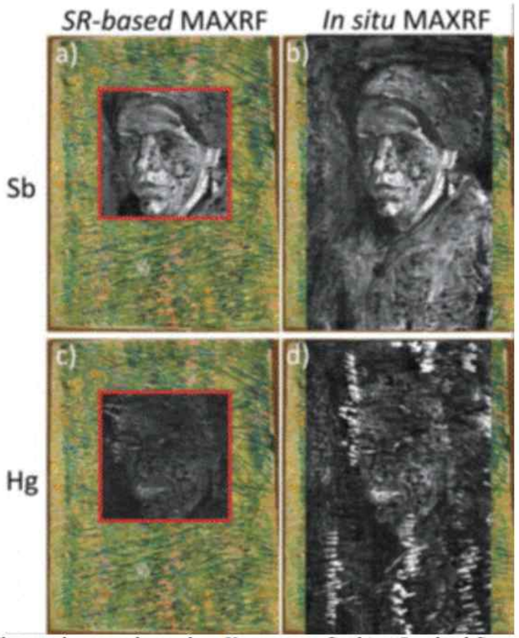

FIG. 8. Elemental maps, obtained on Vincent van Gogh's ''Patch of Grass'', showing the hidden portrait of a woman. (a) and (b) show the Sb distribution, while (c) and (d) show the Hg distribution. (a) and (c) were acquired with MA-XRF at a synchrotron source, while (b) and (d) are results of in situ measurements by means of the mobile scanner. (a) and (c) were acquired with a step size of 0.5 mm and 2 s dwell time in two days, while (b) and (d) were acquired with a step size of 1 mm and a dwell time of 5.1 s in six days.

J. Anal. At. Spectrom., 2011, 26, 899

Phar Lap's preserved hide, which is on display at Museum Victoria, Melbourne, Australia.

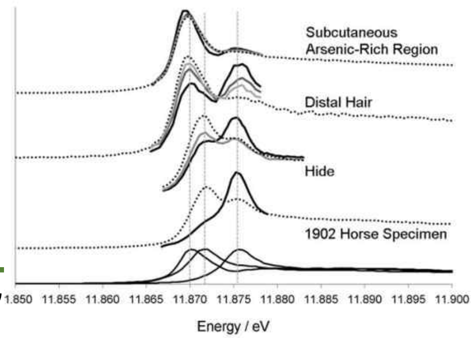

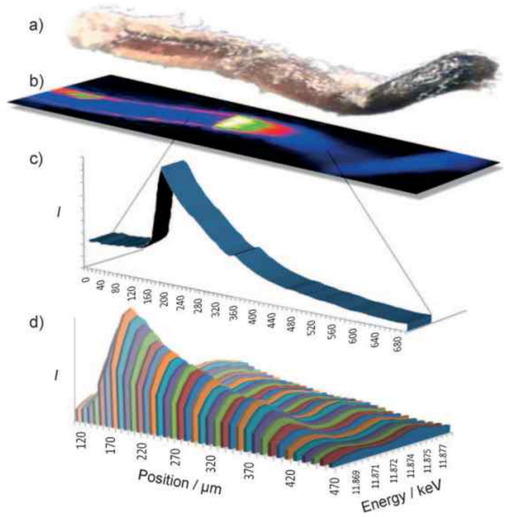

Figure 2. Analysis of Phar Lap's hair. An optical image shows the root end of one hair with the root sheath intact (a). The hair was analyzed with an X-ray microprobe that imaged the internal arsenic distribution (b). The longitudinal profile reflects the hair growing outwards as the arsenic is metabolized (c), while 2D XANES mapping reveals the variation in arsenic speciation ratios (d).

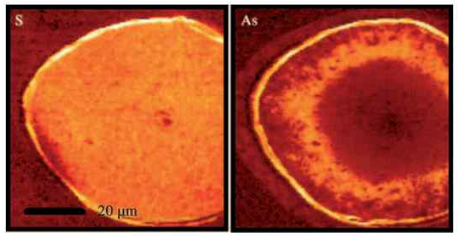

Figure 4. Micro X-ray fluorescence maps of sulfur and arsenic. Arsenic has a strong affinity for the sulfur-rich cuticle layer as well as within the cortex, and to a lesser extent the root sheath.

Angew. Chem. Int. Ed. 2010, 49, 4237

Batteries

✓ In situ/operando synchrotron-based X-ray techniques for lithium-ion battery research

- Lithium-ion battery (LIB) technology
- Challenges such as energy density, cycle life, and safety
- Fundamental understanding of the reaction mechanisms in various physical/chemical processes during LIB operation

- synchrotron-based X-ray characterization techniques are powerful tools for providing valuable information about the complicated reaction mechanisms

❖ Synchrotron based X-ray techniques

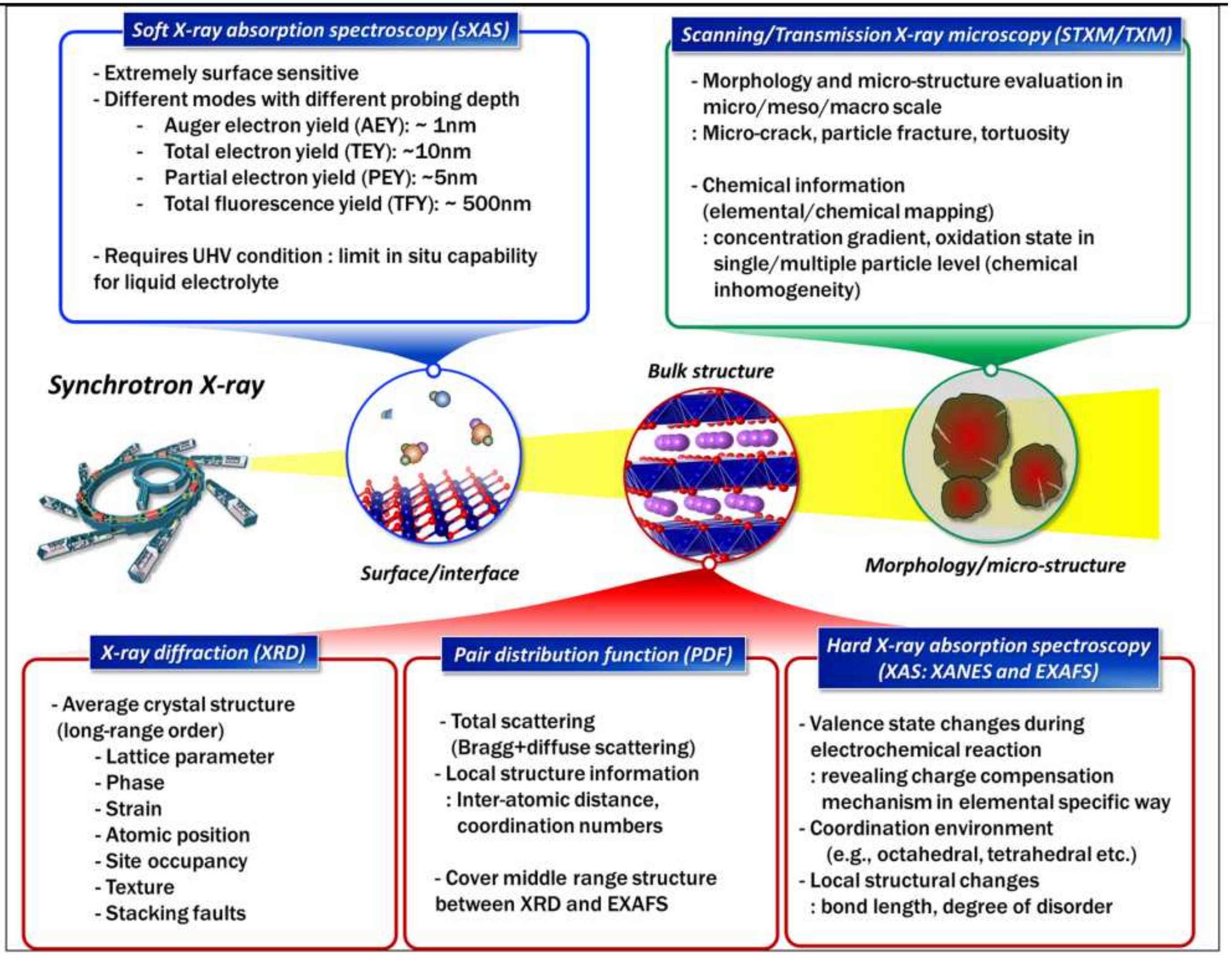

CO Oxidation

➢ **Influence of lattice oxygen on the catalytic activity of blue titania supported Pt catalyst for CO oxidation**

- Characteristics of the active oxygen species of blue TiO_2 with a higher concentration of oxygen vacancies as a model catalyst with deposited nano-sized Pt toward CO oxidation are unraveled
- Surface lattice oxygen of blue TiO2 leads to the high activity of CO oxidation

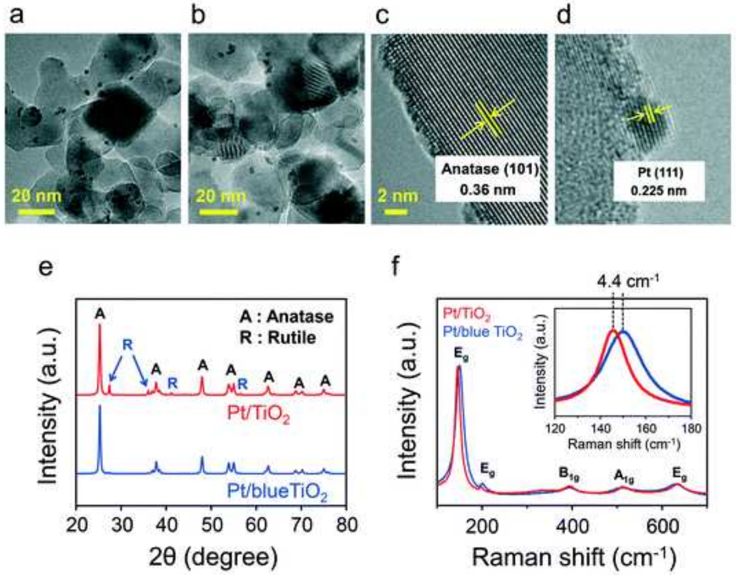

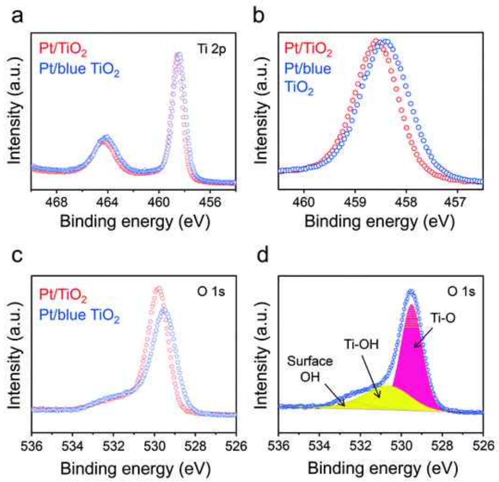

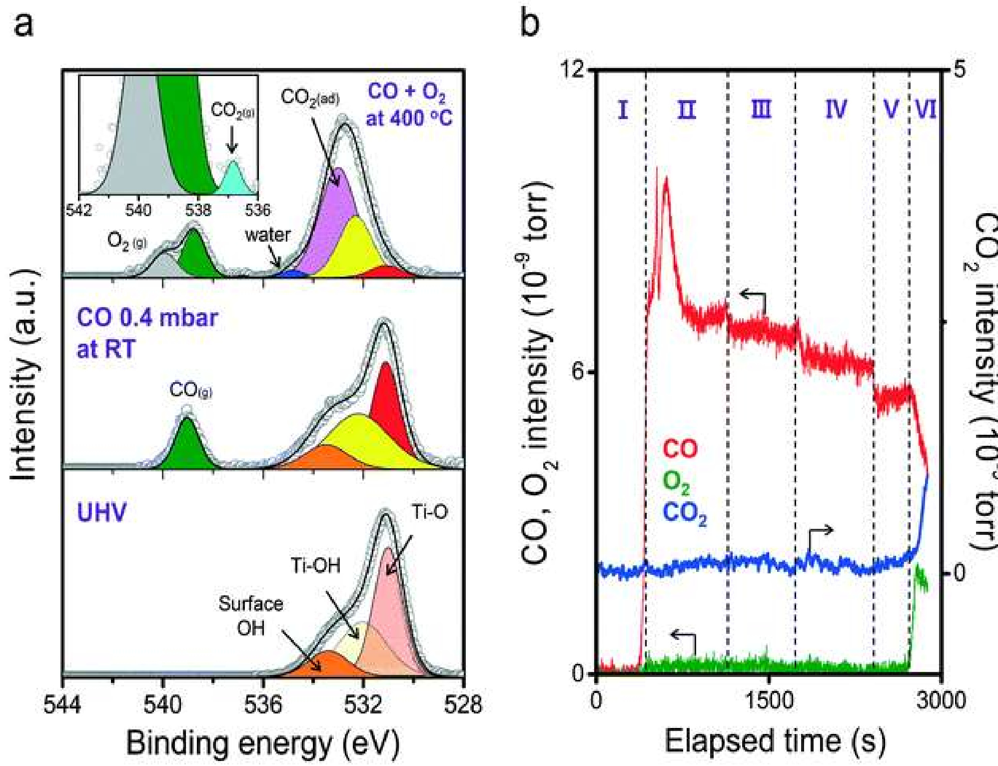

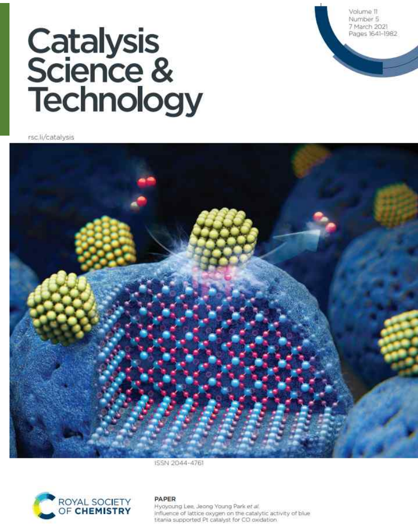

H. Choi, et al., Catal. Sci. Technol., 11, 1698(2021)

❖ In situ XAS to investigate the different contributions of three transition metals to the electrochemical charge/discharge reactions in Li1.2Ni0.15Co0.1Mn0.55O2

❖ In situ XRD of Li2MoO3 and TR-XRD of LiNi1/3Co1/3Mn1/3O2

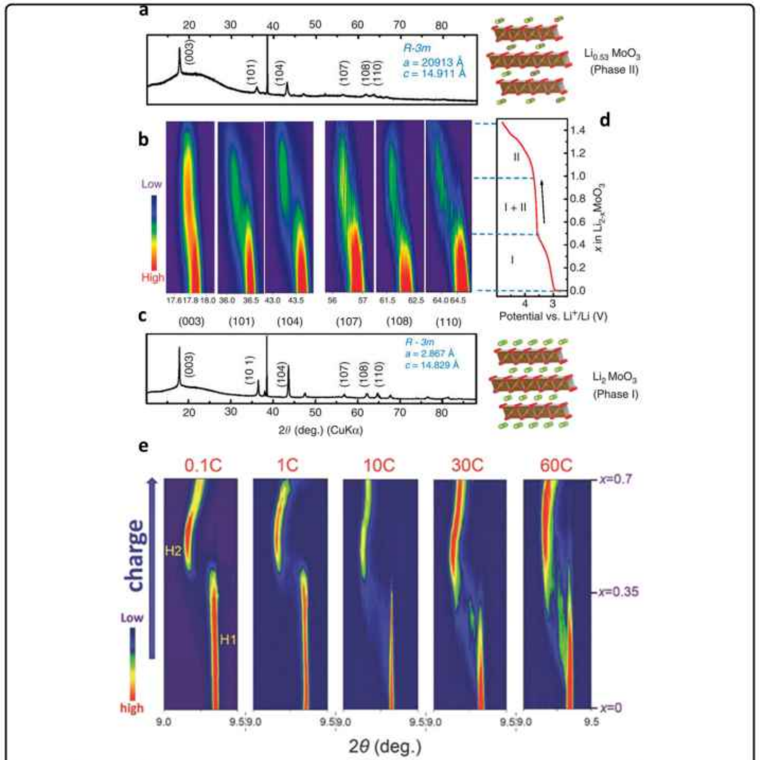

Fig. 3 In situ XRD of Li_2MoO_3 and TR-XRD of $LiNi_{1/3}Co_{1/3}Mn_{1/3}O_2$. **a** The XRD pattern of a $Li_{2-x}MoO_3$ electrode immediately after charging to 4.8 V. **b** Contour plot of the diffraction peak evolution of the (003), (101), (104), (107), (108), and (110) planes during delithiation. **c** The XRD pattern of the Li_2MoO_3 electrode before charging. **d** Charge curve at a current density of 10 mA g^{-1} from the open-circuit voltage (OCV) to 4.8 V during XRD data collection; reproduced with permission[29]. Copyright 2014, Nature Publishing Group. **e** In situ XRD of $LiNi_{1/3}Mn_{1/3}Co_{1/3}O_2$ during the first charge. Contour plot of the (003) diffraction peak of $Li_{1-x}Ni_{1/3}Co_{1/3}Mn_{1/3}O_2$ with as x is increased between $x = 0$ and 0.7 during the first charging process at different C rates (0.1, 1, 10, 30, and 60 C). Data were collected at X14A at NSLS with a wavelength of 0.7747 Å. Reproduced with permission[15]. Copyright 2016, WILEY-VCH

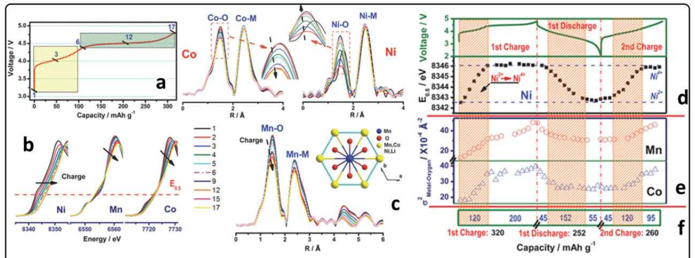

Fig. 6 In situ XAS to investigate the different contributions of three transition metals to the electrochemical charge/discharge reactions in $Li_{1.2}Ni_{0.15}Co_{0.1}Mn_{0.55}O_2$. **a** The first charging curve of $Li_{1.2}Ni_{0.15}Co_{0.1}Mn_{0.55}O_2$ during an in situ XAS experiment (current density: 21 mA g^{-1}). **b** Normalized XANES spectra and **c** the magnitude of the Fourier transformed Mn, Co and Ni K-edge spectra of $Li_{1.2}Ni_{0.5}Co_{0.1}Mn_{0.55}O_2$ collected during the initial charging process. Inset: a schematic view of the coordination environment around the Mn ions. Quantitative correlation of the capacity with respect to reaction sites. Evolution of **d** the half-height energy position of the Ni K-edge XANES spectra and **e** Debye-Waller factors of Mn-O and Co-O during in situ XAS measurements. **f** The capacity delivered in a corresponding voltage range. Reproduced with permission[36]. Copyright 2013, WILEY-VCH

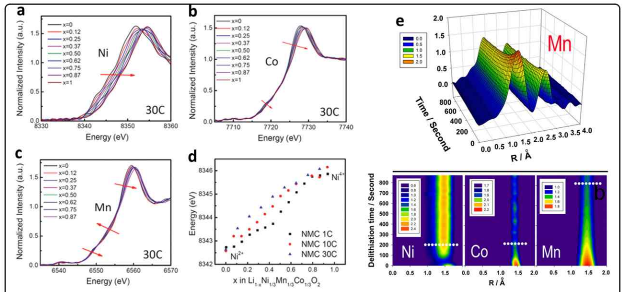

Fig. 7 In situ TR-XAS of $LiNi_{1/3}Mn_{1/3}Co_{1/3}O_2$ and $Li_{1.2}Ni_{0.15}Co_{0.1}Mn_{0.55}O_2$ during constant current charging and constant voltage charging. Normalized XANES spectra of NMC at the **a** Ni, **b** Co, and **c** Mn K-edges during 30 C charging. **d** The Ni K-edge energy shift as a function of nominal lithium content x in $Li_{1-x}Ni_{1/3}Mn_{1/3}Co_{1/3}O_2$ during the initial charge process at the current rates of 1, 10, and 30 C. Reproduced with permission[15]. Copyright 2016, WILEY-VCH. **e** Magnitude of the Fourier transformed Mn K-edge spectra of $Li_{1.2}Ni_{0.15}Co_{0.1}Mn_{0.55}O_2$ collected during charging with a 5 V constant voltage. The projection view of the corresponding Ni–O, Co–O, and Mn–O peak magnitudes of the Fourier transformed K-edge spectra as a function of the charging time. Reproduced with permission[36]. Copyright 2013, WILEY-VCH

❖ Operando sXAS results collected by using a LiNi1/3Mn1/3Co1/3O2 /PEO-LiTFSI/Li battery cell

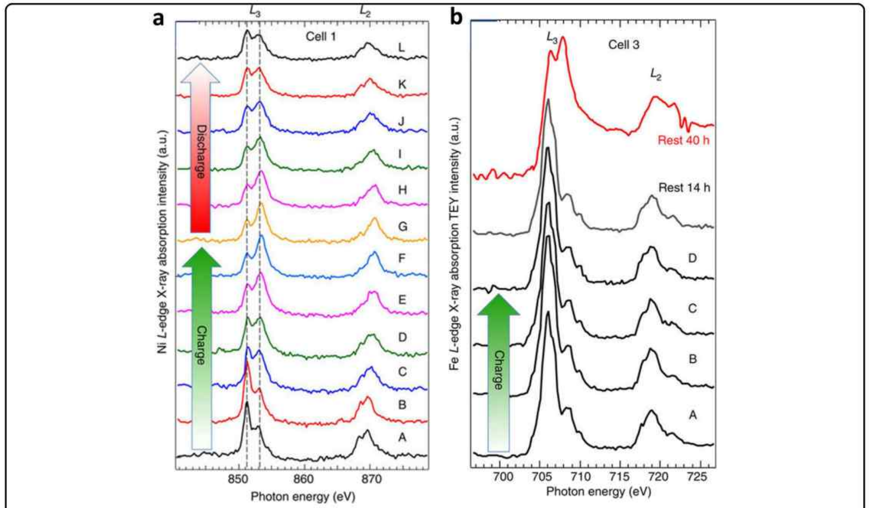

Fig. 8 Operando sXAS results collected by using a $LiNi_{1/3}Mn_{1/3}Co_{1/3}O_2$ /PEO-LiTFSI/Li battery cell. **a** Ni L-edge sXAS TFY spectra of an NMC cathode. Data collected simultaneously with electrochemical cycling at a C/5 rate. **b** Fe L-edge sXAS TEY spectra of the $LiFePO_4$ cathode in Cell 3 at different electrochemical cycling stages labeled A–D in the initial charge cycle and after 14 and 40 h of relaxation. The line shape at L_3 at approximately 706 eV and L_2 at approximately 719 eV fingerprints the oxidation state of Fe in $LiFePO_4$, which does not show any change without long relaxation. Reproduced with permission[13]. Copyright 2013, Nature Publishing Group

Batteries

❖ In situ synchrotron-based X-ray techniques and their capabilities/limitations

Technique		Capability	Limitation	References
X-ray Diffraction (XRD)		- Average structure information : degree of crystallinity, phase purity, phase identification, atomic position, lattice parameter - Relatively easy to design experiments and in situ cells.	Difficult to obtain information for amorphous materials.	11-12,15-16,18,19, 29
X-ray Pair Distribution Function Analysis (XPDF)		- Both short-range and long-range structural information : Atomic pair distance, local ordering/disordering. - Useful to solve structure of amorphous, disordered materials	- Limited resources (few number of capable beamlines) - Require careful in-situ cell design	30-32
X-ray Absorption spectroscopy	Hard X-ray absorption spectroscopy (hXAS)	XANES : valence state changes, covalency, and local coordination environment in elemental specific way EXAFS : local structural changes of bond length, coordination number, degree of disordering	- Not capable to study low atomic number elements	15, 32-39
	Soft X-ray absorption spectroscopy (sXAS)	- Surface sensitive technique to probe electrode materials - Different modes with different probing depth Auger electron yield (AEY): ~ 1 nm Total electron yield (TEY): ~10 nm Partial electron yield (PEY): ~5 nm Total fluorescence yield (TFY): ~ 500 nm	- Requires ultra-high vacuum (UHV) condition for measurement : Difficult to construct in situ cells using liquid electrolyte	13,57
Scanning/Transmission X-ray microscopy (STXM/TXM)		- Morphology and structure evaluation in micro/macro scale : Capable to observe micro-crack, particle fracture, tortuosity - Can obtain chemical information (elemental/chemical mapping) : concentration gradient, valence state in single/multiple particle level (chemical inhomogeneity) - 3D tomography : 3D images can be reconstructed using a series of x-ray images collected at different angles.	- Relatively complicated in situ cell design	14, 17, 20, 40-60

❖ Various in situ/operando electrochemical cell designs for synchrotron-based X-ray characterization

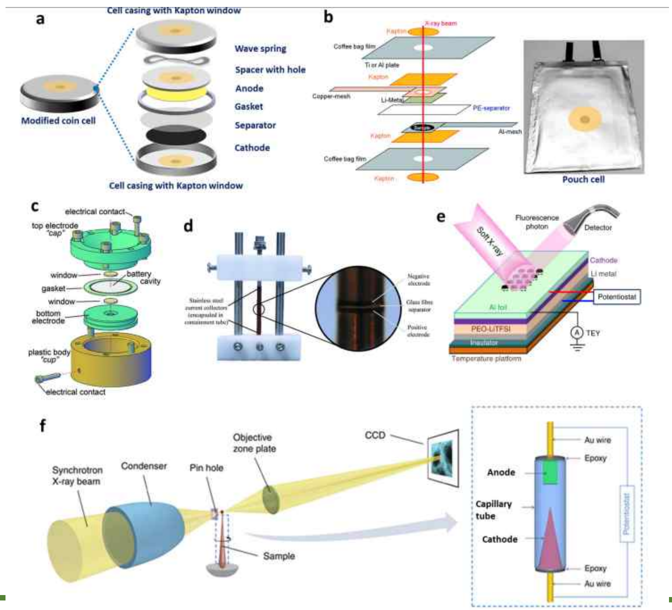

NPG Asia Materials (2018) 10: 563-580

포항가속기연구소(PAL) & Korea-4GSR

- 3세대 방사광가속기인 PLS-II의 성공적인 구축과 운영으로부터, 산업적 활용과 고도화된 연구 수요를 충족하기 위해 4세대 방사광가속기의 필요성이 대두됨
- 다목적방사광가속기(Korea-4GSR)는 4세대 방사광가속기로서 세계최고수준의 방사광 제공 및 활용을 목표로 함.
- PAL은 Korea-4GSR 구축사업의 공동연구기관으로서 가속장치 개발과 초기 빔라인 설계 및 설치를 담당하고 있음.

포항방사광가속기 성과

구축 및 운영

* 포항가속기연구소 전경

글로벌 TOP5
- 3세대 방사광가속기
- 엑스선 자유전자레이저 동시 운영

연구소	국가	3세대 방사광가속기	엑스선 레이저	인력
PAL	한국	PLS-II	PAL-XFEL	223
SLAC	미국	SPEAR-III	LCLS	600
RIKEN	일본	SPring-8	SACLA	450
DESY	독일	PETRA-III	European XFEL	950
PSI	스위스	SLS	SwissFEL	-

* 4세대 엑스선 자유전자레이저 PAL-XFEL 내부

학술적 성과

- Science, nature등 가속기활용 논문 다수 등재 ('22 평균 IF: 12.4)

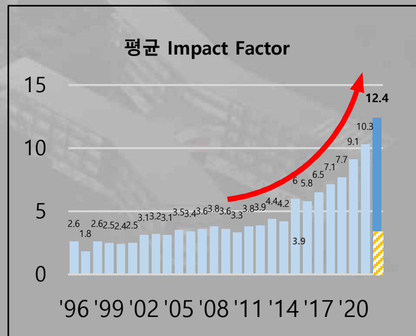

국가 R&D사업 SCIE 논문 평균 Impact Factor 3.9 수준

KBSI 와 PAL이 함께 만드는
대한민국 과학의 밝은 빛

다목적방사광가속기(Korea-4GSR) 구축사업 개요

주관기관: 한국기초과학지원연구원

공동연구기관: 포항가속기연구소

추진주체: 과기정통부/충청북도 청주시

사업기간:
2021.07.01 ~ 2029.12.31

총사업비: 1조 787억원
(국비 8,787억원, 지방비 2,000억원)

부지: 청주시 오창읍 후기리
테크노폴리스 일반산업단지
면적: 540,000㎡
(기본부지 310,000㎡ 포함)
/ 연건평 69,400㎡

저장링 주요 변수	
둘레	798.8 m
빔에너지	4 GeV
빔전류	400 mA
에미턴스	62 pm·rad
광원 크기	약 19 x 6 μm^2
밝기	10^{21} ~ 10^{22} phs/s/mm²/mrad²
결맞음 세기	(@10 keV)~ 10^{13} ph/s/mm²

초기 10기 빔라인 개요

- 산업 우선지원 빔라인
- 연구 지원 빔라인

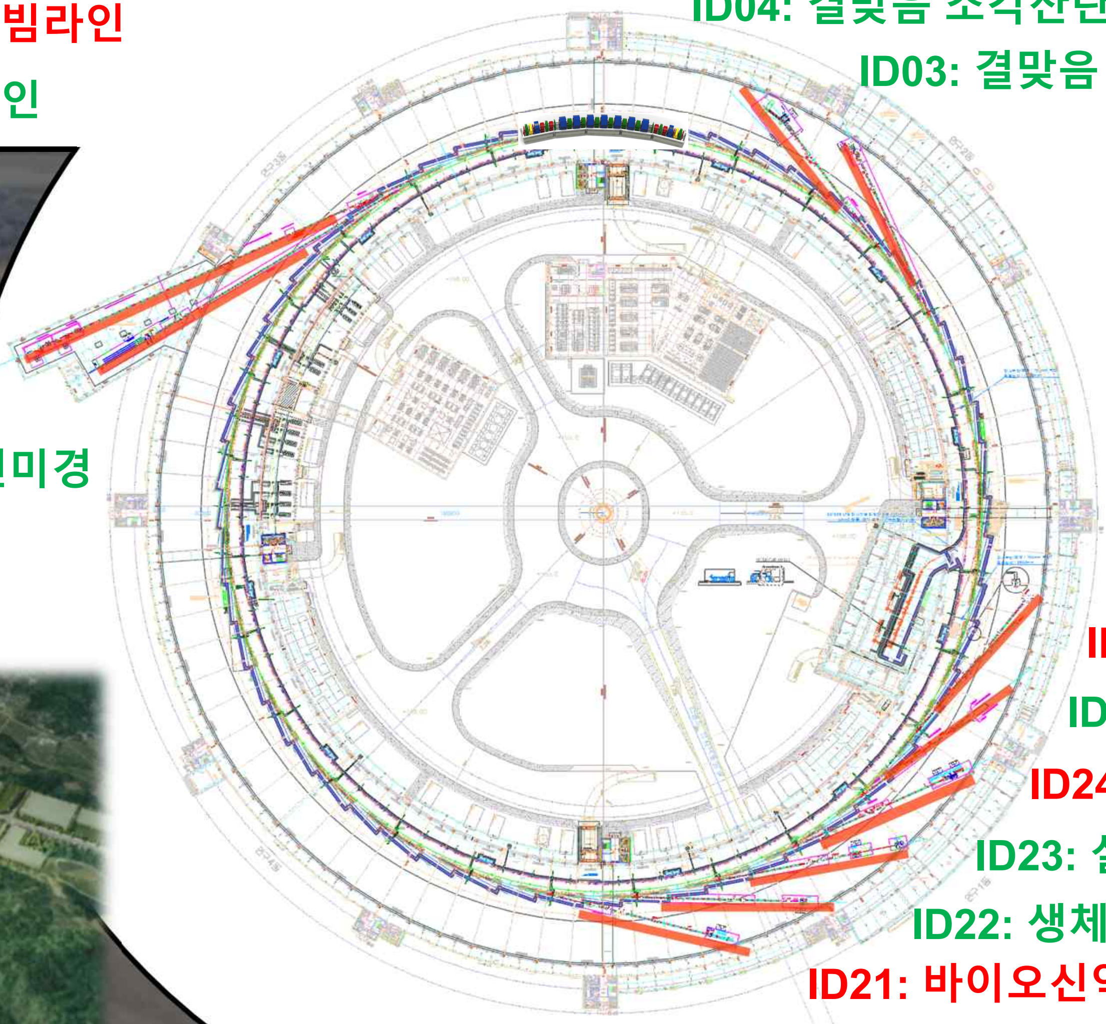

ID04: 결맞음 소각산란

ID03: 결맞음 엑스선 회절

ID10: 나노 탐침

BM10: 고에너지 현미경

ID26: 연엑스선 나노 탐침

ID25 나노 각분해광전자분광

ID24: 소재 구조 분석

ID23: 실시간 흡수분광

ID22: 생체분자 나노결정학

ID21: 바이오신약-바이오소각산란

반도체

에너지 소재

신소재

바이오

화학

환경

지구과학

KBSI 와 PAL이 함께 만드는
대한민국 과학의 밝은 빛

Korea-4GSR 초기 10기 빔라인 사양 개요

	구분	광자 에너지	광원	실험기법	활용분야
산업 우선지원 빔라인	ID21: 바이오신약-바이오소각산란	5~20keV	IVU 24	용액 소각산란	바이오
	ID24: 소재 구조 분석	5 ~40keV	IVU 24	분발회절 & 흡수분광	신소재, 에너지 소재
	ID26: 연엑스선 나노 탐침	0.1~5keV	IVU24 +EPU78	엑스선 광전자 분광법 엑스선 흡수 분광법 주사 광전자 현미경	반도체, 신소재
연구지원 빔라인	ID25: 나노 각분해광전자분광	0.1~2keV	EPU98	각분해 광전자분광	반도체, 신소재
	ID03: 결맞음 엑스선 회절	3~30keV	IVU22	결맞음회절 영상법 엑스선 회절	반도체, 신소재, 지구과학, 화학
	ID04: 결맞음 소각산란	7~30keV	IVU20	소각산란/광각산란 엑스선 광자 상관 분광법	신소재, 화학
	ID23: 실시간 흡수분광	4~40keV	IVU 24	엑스선 광전자 분광법 엑스선 흡수 분광법	신소재, 환경, 지구과학, 화학
	ID22: 생체분자 나노결정학	8~25keV	IVU20	나노결정구조	바이오
	BM10: 고에너지 현미경	5~100keV	BM	투영 영상법	신소재, 에너지 소재, 바이오
	ID10: 나노 탐침	5~25keV	IVU24	주사형 회절 영상법 엑스선 형광 현미경 단층 촬영법	반도체, 에너지 소재, 지구과학, 화학, 환경